Chapter 10
Kinematics of Alternative Robotic Mechanical Systems

10.1 Introduction

The study of robotic mechanical systems has focused, so far, on serial manipulators. These are the most common systems of their kind, but nowadays by no means the majority. In recent years, other kinds of robotic mechanical systems have been developed, as outlined in Chap. 1. Under *alternative robotic mechanical systems* we understand here: (a) parallel robots; (b) multifingered hands; (c) walking machines; and (d) rolling robots. A class that is increasingly receiving attention, *humanoids*, portrays an architecture inspired from the human musculo-skeletal system. This class deserves a study on its own because of the host of control problems that it poses to the roboticist; its kinematics, however, can be studied with the tools developed in this chapter for the first three kinds of systems listed above. For this reason, a section on humanoids is not included here.

Moreover, under the general heading of *kinematics*, we study in this chapter the geometry and velocity relations between the sets of joint and Cartesian variables. For the sake of brevity, however, we leave aside the statics of these systems. The reader should be able to derive these relations from the duality between kinematics and statics, as outlined in Chaps. 3 and 5. Some exercises in this regard are included in this chapter.

10.2 Kinematics of Parallel Manipulators

Unlike serial manipulators, their parallel counterparts are composed of kinematic chains with closed subchains. A fairly general parallel manipulator is shown in Fig. 10.1, in which one can distinguish two platforms, one fixed to the ground, $\mathcal{B}$, and one capable of moving arbitrarily within its workspace, $\mathcal{M}$. The moving

J. Angeles, *Fundamentals of Robotic Mechanical Systems: Theory, Methods, and Algorithms*, Mechanical Engineering Series 124, DOI 10.1007/978-3-319-01851-5_10,

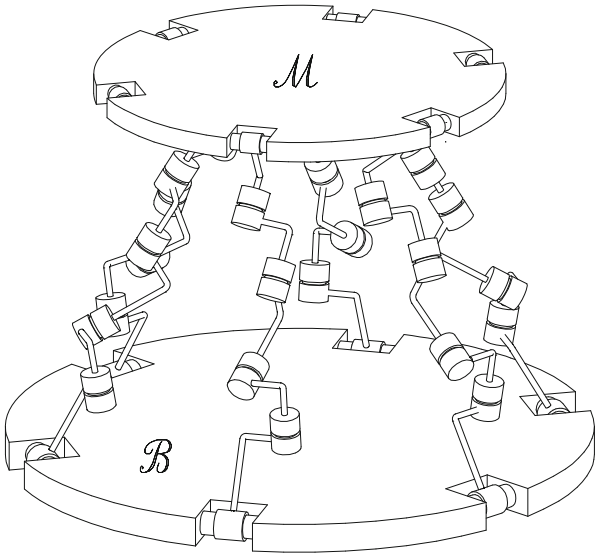

Fig. 10.1 A general six-dof parallel manipulator

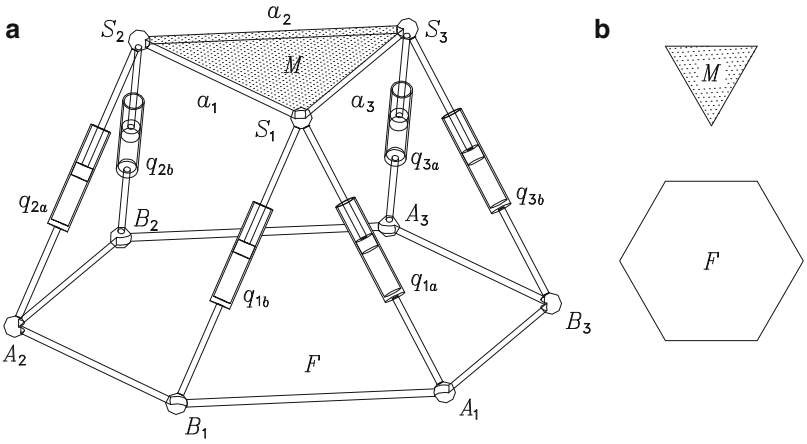

Fig. 10.2 A six-dof flight simulator: (**a**) general layout; (**b**) geometry of its two platforms

platform is connected to the fixed platform through six *legs*, each being regarded as a six-axis serial manipulator whose base is $\mathcal{B}$ and whose end-effector is $\mathcal{M}$. The whole leg is composed of six links coupled through six revolutes.

The robotic architecture shown in Fig. 10.1 is, in fact, too general, and of little use as such. A simpler and more practical parallel architecture, which is used as a flight simulator, is sketched in Fig. 10.2a. In this figure, the fixed platform $\mathcal{B}$ is a regular hexagon, while the moving platform $\mathcal{M}$ is an equilateral triangle, as depicted in Fig. 10.2b. Moreover, $\mathcal{B}$ is connected to $\mathcal{M}$ by means of six serial chains,

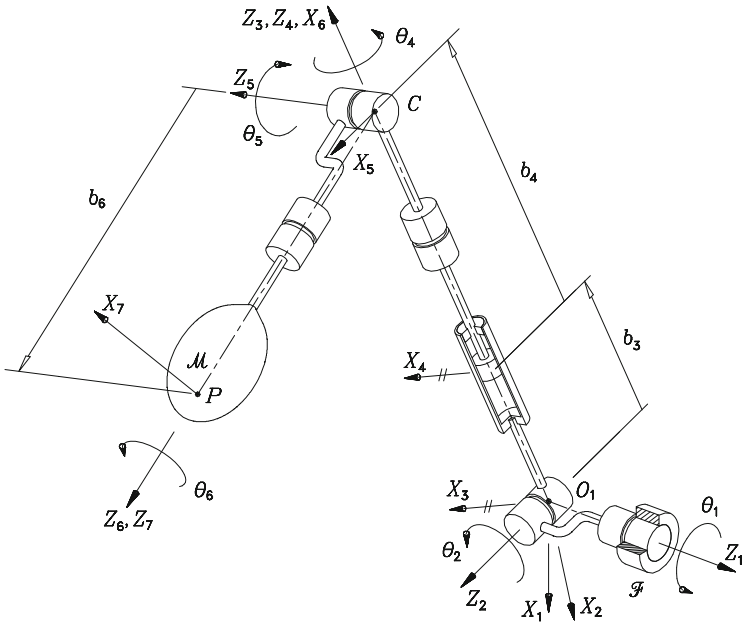

Fig. 10.3 A layout of a leg of the manipulator of Fig. 10.2

each comprising five revolutes and one prismatic pair. Three of the revolutes bear concurrent axes, and hence, constitute a spherical joint, similar to the wrists studied in Sect. 4.4, while two more have axes intersecting at right angles, thus constituting a *universal joint*. Of the six foregoing joints, only one, the prismatic pair, is actuated.

It is to be noted that although each leg of the manipulator of Fig. 10.2a has a spherical joint at only one end and a universal joint at the other end, we represent each leg in that figure with a spherical joint at each end. Kinematically, the leg depicted in Fig. 10.2a is equivalent to the actual one, the only difference being that the former appears to have a redundant joint. We use the model of Fig. 10.2a only to make the drawing simpler. A more accurate display of the leg architecture of this manipulator appears in Fig. 10.3.

Because the kinematics and statics of parallel manipulators at large are beyond the scope of this book, we will limit the discussion to parallel manipulators of the simplest type.

With regard to the manipulators under study, we can also distinguish between the inverse and the direct kinematics problems in exactly the same way as these problems were defined for serial manipulators. The inverse kinematics of the general manipulator of Fig. 10.1 is identical to that of the general serial manipulator studied in Sect. 9.2. In fact, each leg can be studied separately for this purpose, the problem thus becoming the same as in that section. For the particular architecture of the manipulator of Fig. 10.2a, in which the actuated joint variables are displacements measured along the leg axes, the inverse kinematics simplifies substantially and

allows for a simple closed-form solution. However, the direct kinematics of the same manipulator is as challenging as that of the general serial manipulator of Sect. 9.2. With regard to the direct kinematics of manipulators of the type depicted in Fig. 10.2a, Charentus and Renaud (1989) and Nanua et al. (1990) showed independently that like the inverse kinematics of general six-axis serial manipulators, the direct kinematics of this manipulator reduces to a 16th-degree polynomial. Note, however, that the direct kinematics of a manipulator similar to that of Fig. 10.2a, but with arbitrary locations of the attachment points of each leg to the moving and fixed platforms, termed the *general platform manipulator*, has been the subject of intensive research (Merlet 2006). A breakthrough in the solution of the direct kinematics of platform manipulators of the general type was reported by Raghavan (1993), who resorted to polynomial continuation, a technique already mentioned in Sect. 9.2, for computing up to 40 poses of $\mathcal{M}$ for given leg lengths of a parallel manipulator with legs of the type depicted in Fig. 10.3, but with attachment points at both $\mathcal{M}$ and $\mathcal{B}$ with an arbitrary layout. What Raghavan did not derive is the characteristic 40th-degree polynomial of the general platform manipulator. Independently, Wampler (1996) and Husty (1996) devised procedures to derive this polynomial, although Wampler did not pursue the univariate polynomial approach and preferred to cast the problem in a form suitable for its solution by means of polynomial continuation. Husty did derive the 40th-degree polynomial for several examples. In the process, he showed that this polynomial is the underlying characteristic polynomial for all manipulators of the platform type, which simplifies to a lower-degree polynomial for simpler architectures. As a matter of fact, Lee and Roth (1993) solved the direct kinematics of platform manipulators for which the attachment points at the base and the moving platforms are located at the vertices of planar, similar hexagons. These researchers showed that the problem here reduces to a cascade of quadratic and linear equations. In the particular case in which both polygons are regular, however, the manipulator degenerates into a movable structure, upon fixing the leg lengths, and hence, the solution set becomes a continuum. Lazard and Merlet (1994), in turn, showed that the platform manipulator originally proposed by Stewart (1965), and known as the *Stewart–Gough platform*, has a 12th-degree characteristic polynomial. Interestingly, these mechanical systems were first introduced by Gough (1956–1957) for testing tires; Stewart (1965) suggested their use as flight simulators, an application that is now well established.

Husty, however, did not show that his 40th-degree polynomial is minimal in that manipulator architectures are possible that exhibit up to 40 actual solutions. Dietmaier (1998) did this, by devising an algorithm that would iteratively increase the number of real solutions of a given architecture. With this paper, Dietmaier proved conclusively that Husty's 40th-degree polynomial is, in fact, minimal. This was rather surprising, for virtually everybody working in the field expected a minimal polynomial of a degree of the form 2^n, with n being a positive integer. Notice that, in the cases of the most general serial six-revolute manipulator and of the flight simulator, the minimal polynomial is of a degree of this form, with $n = 4$.

Table 10.1 DH parameters of the leg of Fig. 10.3

i	a_i	b_i	α_i
1	0	0	90°
2	0	0	90°
3	0	b_3	0°
4	0	b_4 (const)	90°
5	0	0	90°
6	0	b_6 (const)	0°

Below we analyze the inverse kinematics of one leg of the manipulator of Fig. 10.2a, as depicted in Fig. 10.3. The Denavit–Hartenberg parameters of the leg shown in this figure are given in Table 10.1. It is apparent that the leg under study is a decoupled manipulator. Its inverse kinematics can be derived by properly modifying the scheme introduced in Sect. 4.4, for we now have a prismatic joint, which is, in fact, the only active joint of this manipulator. Moreover, by virtue of the underlying design, the active joint variable, b_3, can take on only positive values.

In view of the DH parameters of this manipulator, Eq. (4.16) reduces to

$$\mathbf{Q}_1\mathbf{Q}_2(\mathbf{a}_3 + \mathbf{a}_4) = \mathbf{c} \tag{10.1}$$

where $\mathbf{c}$ denotes the position vector of the center C of the spherical wrist and, since frames $\mathcal{F}_3$ and $\mathcal{F}_4$ of the DH notation are related by a pure translation, $\mathbf{Q}_3 = \mathbf{1}$. Upon equating the squares of the Euclidean norms of both sides of the foregoing equation, we obtain

$$\|\mathbf{a}_3 + \mathbf{a}_4\|^2 = \|\mathbf{c}\|^2 \tag{10.2}$$

where, by virtue of the DH parameters of Table 10.1,

$$\|\mathbf{a}_3 + \mathbf{a}_4\|^2 = (b_3 + b_4)^2$$

Now, since both b_3 and b_4 are positive by construction, Eq. (10.2) readily leads to the desired inverse kinematics solution, namely,

$$b_3 = \|\mathbf{c}\| - b_4 > 0 \tag{10.3}$$

a result that could have been derived by inspection of Fig. 10.3.

Note that the remaining five joint variables of the leg under study are not needed for purposes of inverse kinematics, and hence, their calculation could be skipped. However, in studying the differential kinematics of these manipulators, these variables will be needed; it is thus convenient to solve for them now. This is straightforward, as shown below: Upon expansion of Eq. (10.1), we derive three scalar equations in two unknowns, θ_1 and θ_2, namely,

$$(b_3 + b_4)s_2 = x_C c_1 + y_C s_1 \tag{10.4a}$$

$$-(b_3 + b_4)c_2 = z_C \tag{10.4b}$$

$$0 = x_C s_1 - y_C c_1 \tag{10.4c}$$

in which c_i and s_i stand for $\cos\theta_i$ and $\sin\theta_i$, respectively, while b_3, occurring in the above equations, is available in Eq. (10.3). From Eq. (10.4c), θ_1 is derived as

$$\theta_1 = \tan^{-1}\left(\frac{y_C}{x_C}\right) \tag{10.5a}$$

which yields a unique value of θ_1 rather than the two lying π radians apart, for the two coordinates x_C and y_C determine the quadrant in which θ_1 lies. Once θ_1 is known, θ_2 is derived uniquely from the remaining two equations through its cosine and sine functions, i.e.,

$$c_2 = -\frac{z_C}{b_3 + b_4}, \quad s_2 = \frac{x_C c_1 + y_C s_1}{b_3 + b_4} \tag{10.5b}$$

With the first three joint variables of this leg known, the remaining ones, i.e., those of the "wrist," are calculated as described in Sect. 4.4.2. Therefore, the inverse kinematics of each leg admits two solutions, one for the first three variables and two for the last three. Moreover, since the only actuated joint is one of the first three, which of the two wrist solutions is chosen does not affect the value of b_3, and hence, each manipulator leg admits only one inverse kinematics solution.

While the inverse kinematics of this leg is quite straightforward, its direct kinematics is not. Below we give an outline of the solution procedure for the manipulator under study that follows the procedure proposed by Nanua et al. (1990).

In Fig. 10.2a, consider the triangles $A_i S_i B_i$, for $i = 1, 2, 3$, where the subscript i stands for the ith pair of legs. When the lengths of the six legs are fixed and plate $\mathcal{M}$ is removed, triangle $A_i S_i B_i$ can only rotate about the axis $A_i B_i$. Therefore, we can replace the pair of legs of lengths q_{ia} and q_{ib} by a single leg of length l_i, connected to the base plate $\mathcal{B}$ by a revolute joint with its axis along $A_i B_i$. The resulting simplified structure, as shown in Fig. 10.4, is kinematically equivalent to the original structure in Fig. 10.2a.

Now we introduce the coordinate frame $\mathcal{F}_i$, with origin at the attachment point O_i of the ith leg with the base plate $\mathcal{B}$, according with the geometry of Fig. 10.4 and the notation below:
For $i = 1, 2, 3$,

X_i is directed from A_i to B_i;
Y_i is chosen such that Z_i is perpendicular to the plane of the hexagonal base and points upwards.
O_i is set at the intersection of X_i and Y_i, and is designated the center of the revolute joint;

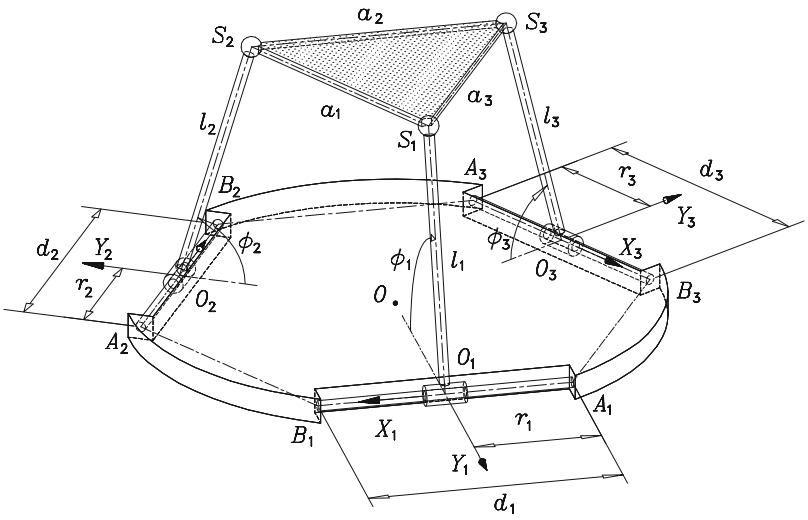

Fig. 10.4 Equivalent simplified mechanism

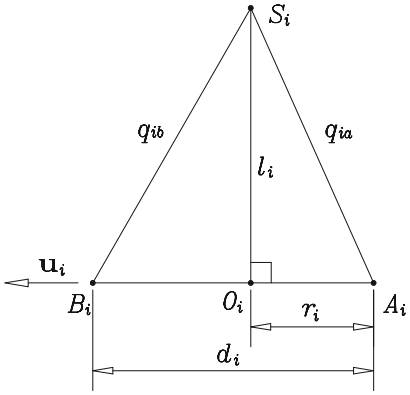

Fig. 10.5 Replacing each pair of legs with a single leg

Next, we locate the three vertices S_1, S_2, and S_3 of the triangular plate with position vectors stemming from the center O of the hexagon. Furthermore, we need to determine l_i and O_i. Referring to Figs. 10.4 and 10.5, and letting $\mathbf{a}_i$ and $\mathbf{b}_i$ denote the position vectors of points A_i and B_i, respectively, we have

$$
\begin{aligned}
d_i &= \|\mathbf{b}_i - \mathbf{a}_i\| \\
r_i &= \frac{d_i^2 + q_{ia}^2 - q_{ib}^2}{2d_i} \\
l_i &= \sqrt{q_{ia}^2 - r_i^2} \\
\mathbf{u}_i &= \frac{\mathbf{b}_i - \mathbf{a}_i}{d_i}
\end{aligned}
$$

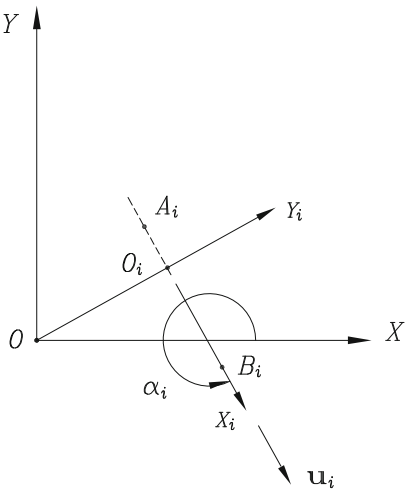

Fig. 10.6 Relation between frames $\mathcal{F}_0$ and $\mathcal{F}_i$

for $i = 1, 2, 3$, and hence, $\mathbf{u}_i$ is the unit vector directed from A_i to B_i. Moreover, the position of the origin O_i is given by vector $\mathbf{o}_i$, as indicated below:

$$\mathbf{o}_i = \mathbf{a}_i + r_i \mathbf{u}_i, \qquad \text{for } i = 1, 2, 3. \tag{10.6}$$

Furthermore, let $\mathbf{s}_i$ be the position vector of S_i in frame $\mathcal{F}_i$ (O_i, X_i, Y_i, Z_i). Then

$$\mathbf{s}_i = \begin{bmatrix} 0 \\ -l_i \cos\phi_i \\ l_i \sin\phi_i \end{bmatrix}, \qquad \text{for } i = 1, 2, 3 \tag{10.7}$$

Now a frame $\mathcal{F}_0\,(O, X, Y, Z)$ is defined with origin at O and axes X and Y in the plane of the base hexagon, and related to X_i and Y_i as depicted in Fig. 10.6. When expressed in frame $\mathcal{F}_0$, $\mathbf{s}_i$ takes on the form

$$[\,\mathbf{s}_i\,]_0 = [\,\mathbf{o}_i\,]_0 + [\,\mathbf{R}_i\,]_0 \mathbf{s}_i, \qquad \text{for } i = 1, 2, 3 \tag{10.8}$$

where $[\,\mathbf{R}_i\,]_0$ is the matrix that rotates frame $\mathcal{F}_0$ to frame $\mathcal{F}_i$, expressed in $\mathcal{F}_0$, and is given as

$$[\,\mathbf{R}_i\,]_0 = \begin{bmatrix} \cos\alpha_i & -\sin\alpha_i & 0 \\ \sin\alpha_i & \cos\alpha_i & 0 \\ 0 & 0 & 1 \end{bmatrix}, \qquad \text{for } i = 1, 2, 3 \tag{10.9}$$

Referring to Fig. 10.6,

$$\cos\alpha_i = \mathbf{u}_i \cdot \mathbf{i} = u_{ix} \tag{10.10}$$

$$\sin\alpha_i = \mathbf{u}_i \cdot \mathbf{j} = u_{iy} \tag{10.11}$$

After substitution of Eqs. (10.9)–(10.11) into Eq. (10.8), we obtain

$$[\,\mathbf{s}_i\,]_0 = [\,\mathbf{o}_i\,]_0 + l_i \begin{bmatrix} u_{iy}\cos\phi_i \\ -u_{ix}\cos\phi_i \\ \sin\phi_i \end{bmatrix}, \qquad \text{for } i = 1, 2, 3 \tag{10.12}$$

where $\mathbf{o}_i$ is given by Eq. (10.6).

Since the distances between the three vertices of the triangular plate are fixed, the position vectors $\mathbf{s}_1, \mathbf{s}_2$, and $\mathbf{s}_3$ must satisfy the constraints below:

$$\|\mathbf{s}_2 - \mathbf{s}_1\|^2 = a_1^2 \tag{10.13a}$$

$$\|\mathbf{s}_3 - \mathbf{s}_2\|^2 = a_2^2 \tag{10.13b}$$

$$\|\mathbf{s}_1 - \mathbf{s}_3\|^2 = a_3^2 \tag{10.13c}$$

After expansion, Eqs. (10.13a–c) take the forms:

$$D_1 c\phi_1 + D_2 c\phi_2 + D_3 c\phi_1 c\phi_2 + D_4 s\phi_1 s\phi_2 + D_5 = 0 \tag{10.14a}$$

$$E_1 c\phi_2 + E_2 c\phi_3 + E_3 c\phi_2 c\phi_3 + E_4 s\phi_2 s\phi_3 + E_5 = 0 \tag{10.14b}$$

$$F_1 c\phi_1 + F_2 c\phi_3 + F_3 c\phi_1 c\phi_3 + F_4 s\phi_1 s\phi_3 + F_5 = 0 \tag{10.14c}$$

where $c(\cdot)$ and $s(\cdot)$ stand for $\cos(\cdot)$ and $\sin(\cdot)$, respectively, while coefficients $\{D_i, E_i, F_i\}_1^5$ are functions of the data only and bear the forms shown below[1]:

$$\begin{aligned} D_1 &= 2l_1(\mathbf{o}_2 - \mathbf{o}_1)^T \mathbf{E}\mathbf{u}_1 \\ D_2 &= -2l_2(\mathbf{o}_2 - \mathbf{o}_1)^T \mathbf{E}\mathbf{u}_2 \\ D_3 &= -2l_1 l_2 \mathbf{u}_2^T \mathbf{u}_1 \\ D_4 &= -2l_1 l_2 \\ D_5 &= \|\mathbf{o}_2\|^2 + \|\mathbf{o}_1\|^2 - 2\mathbf{o}_1^T \mathbf{o}_2 + l_1^2 + l_2^2 - a_1^2 \end{aligned}$$

$$\begin{aligned} E_1 &= 2l_2(\mathbf{o}_3 - \mathbf{o}_2)^T \mathbf{E}\mathbf{u}_2 \\ E_2 &= -2l_3(\mathbf{o}_3 - \mathbf{o}_2)^T \mathbf{E}\mathbf{u}_3 \\ E_3 &= -2l_2 l_3 \mathbf{u}_3^T \mathbf{u}_2 \\ E_4 &= -2l_2 l_3 \\ E_5 &= \|\mathbf{o}_3\|^2 + \|\mathbf{o}_2\|^2 - 2\mathbf{o}_3^T \mathbf{o}_2 + l_2^2 + l_3^2 - a_2^2 \end{aligned}$$

[1]Since all vectors in the 15 coefficients of interest are coplanar, they are regarded as two-dimensional vectors in the display of the 15 coefficients.

$$
\begin{aligned}
F_1 &= 2l_1(\mathbf{o}_1 - \mathbf{o}_3)^T \mathbf{E}\mathbf{u}_1 \\
F_2 &= -2l_3(\mathbf{o}_1 - \mathbf{o}_3)^T \mathbf{E}\mathbf{u}_3 \\
F_3 &= -2l_1 l_3 \mathbf{u}_3^T \mathbf{u}_1 \\
F_4 &= -2l_1 l_3 \\
F_5 &= \|\mathbf{o}_3\|^2 + \|\mathbf{o}_1\|^2 - 2\mathbf{o}_3^T \mathbf{o}_1 + l_1^2 + l_3^2 - a_3^2
\end{aligned}
$$

In the above relations the 2×2 matrix $\mathbf{E}$ is defined as in Eq. (5.55), and the frame in which the vectors are expressed is immaterial, as long as all vectors appearing in the same scalar product are expressed in the same frame. Since expressions for these vectors in $\mathcal{F}_0$ have already been derived, it is just simpler to perform those computations in this frame.

Our next step is to reduce the foregoing system of three equations in three unknowns to two equations in two unknowns, and hence, obtain two contours in the plane of two of the three unknowns, the desired solutions being determined as the intersections of the two contours. Since Eq. (10.14a) is already free of ϕ_3, all we have to do is eliminate ϕ_3 from equations (10.14b) and (10.14c). To do this, we resort to the usual trigonometric identities relating $c\phi_3$ and $s\phi_3$ with $\tan(\phi_3/2)$, in Eqs. (10.14b) and (10.14c). After we have cleared the denominators by multiplying the two foregoing equations by $(1 + \tau_3^2)$, the equations thus resulting take on the forms

$$k_1\tau_3^2 + k_2\tau_3 + k_3 = 0 \tag{10.15a}$$

$$m_1\tau_3^2 + m_2\tau_3 + m_3 = 0 \tag{10.15b}$$

where k_1, k_2, and k_3 are linear combinations of $s\phi_2$, $c\phi_2$, and 1. Likewise, m_1, m_2, and m_3 are linear combinations of $s\phi_1$, $c\phi_1$, and 1, namely,

$$
\begin{aligned}
k_1 &= E_1 c\phi_2 - E_2 - E_3 c\phi_2 + E_5 \\
k_2 &= 2E_4 s\phi_2 \\
k_3 &= E_1 c\phi_2 + E_2 + E_3 c\phi_2 + E_5 \\
m_1 &= F_1 c\phi_1 - F_2 - F_3 c\phi_1 + F_5 \\
m_2 &= 2F_4 s\phi_1 \\
m_3 &= F_1 c\phi_1 + F_2 + F_3 c\phi_1 + F_5
\end{aligned}
$$

Next, we eliminate τ_3 from the above equations dialytically, as we did in Sect. 5.4.1 to find the workspace of a three-axis serial manipulator. We proceed now by multiplying each of the above equations by τ_3 to obtain two more equations, namely,

$$k_1\tau_3^3 + k_2\tau_3^2 + k_3\tau_3 = 0 \tag{10.15c}$$

$$m_1\tau_3^3 + m_2\tau_3^2 + m_3\tau_3 = 0 \tag{10.15d}$$

Further, we write Eqs. (10.15a)–(10.15d) in homogeneous form:

$$\mathbf{\Phi}\boldsymbol{\tau}_3 = \mathbf{0} \tag{10.16a}$$

with the 4×4 matrix $\mathbf{\Phi}$ and the four-dimensional vector $\boldsymbol{\tau}_3$ defined as

$$\mathbf{\Phi} \equiv \begin{bmatrix} k_1 & k_2 & k_3 & 0 \\ m_1 & m_2 & m_3 & 0 \\ 0 & k_1 & k_2 & k_3 \\ 0 & m_1 & m_2 & m_3 \end{bmatrix}, \quad \boldsymbol{\tau}_3 \equiv \begin{bmatrix} \tau_3^3 \\ \tau_3^2 \\ \tau_3 \\ 1 \end{bmatrix} \tag{10.16b}$$

Equation (10.16a) constitutes a linear homogeneous system. Moreover, in view of the form of vector $\boldsymbol{\tau}_3$, we are interested only in nontrivial solutions, which exist only if $\det(\mathbf{\Phi})$ vanishes. We thus have the condition

$$\det(\mathbf{\Phi}) = 0 \tag{10.16c}$$

Equations (10.14a) and (10.16c) form a system of two equations in two unknowns, ϕ_1 and ϕ_2. These two equations can be further reduced to a single 16th-degree polynomial equation (Nanua et al. 1990), as discussed later on.

In the spirit of the contour method introduced earlier, we plot these two equations as two contours in the ϕ_1–ϕ_2 plane and determine the desired solutions at points where the two contours intersect. Once a pair of (ϕ_1, ϕ_2) values is found, ϕ_3 can be uniquely determined from Eqs. (10.14b and c). Indeed, these equations can be arranged in the form:

$$\begin{bmatrix} E_4 s\phi_2 & E_2 + E_3 c\phi_2 \\ F_4 s\phi_1 & F_2 + F_3 c\phi_1 \end{bmatrix} \begin{bmatrix} s\phi_3 \\ c\phi_3 \end{bmatrix} = \begin{bmatrix} -E_1 c\phi_2 - E_5 \\ -F_1 c\phi_1 - F_5 \end{bmatrix}$$

From the above equation, both $c\phi_3$ and $s\phi_3$ can be found *uniquely*; with the foregoing unique values, ϕ_3 is determined uniquely as well.

Knowing the angles ϕ_1, ϕ_2, and ϕ_3 allows us to determine the position vectors of the three vertices of the mobile plate, $\mathbf{s}_1$, $\mathbf{s}_2$, and $\mathbf{s}_3$, whose expressions are given by Eq. (10.12). Since three points define a plane, the pose of the end-effector is uniquely determined by the positions of its three vertices. We illustrate the foregoing procedure with a numerical example below:

Example 10.2.1 (A Contour-Intersection Approach). We derive the direct kinematics of a manipulator analyzed by Nanua et al. (1990). This is a platform manipulator whose base plate has six vertices with coordinates expressed with respect to the fixed reference frame $\mathcal{F}_0$ as given below, with all data given in meters:

$$A_1 = (-2.9, -0.9)\,, \qquad B_1 = (-1.2,\ \ 3.0)$$
$$A_2 = (\ \ 2.5,\ \ 4.1)\,, \qquad B_2 = (\ \ 3.2,\ \ 1.0)$$
$$A_3 = (\ \ 1.3, -2.3)\,, \qquad B_3 = (-1.2, -3.7)$$

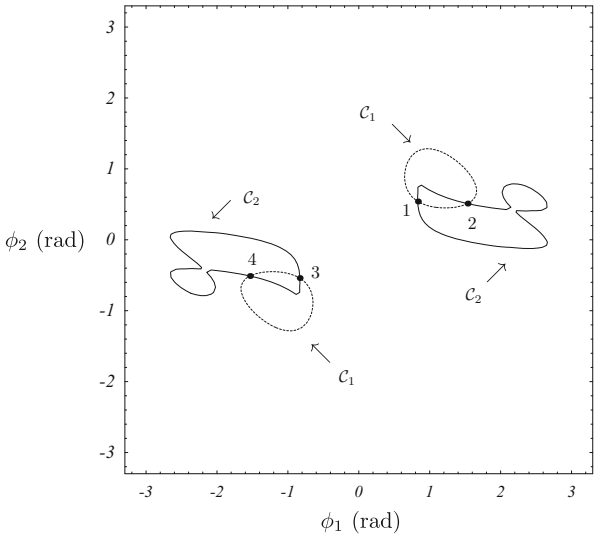

Fig. 10.7 Contours $\mathcal{C}_1$ and $\mathcal{C}_2$ for Nanua et al.'s example

The dimensions of the movable triangular plate are, in turn,

$$a_1 = 2.0, \qquad a_2 = 2.0, \qquad a_3 = 3.0$$

Determine all possible poses of the moving plate for the six leg-lengths given as

$$q_{1a} = 5.0, \quad q_{2a} = 5.5, \quad q_{3a} = 5.7,$$
$$q_{1b} = 4.5, \quad q_{2b} = 5.0, \quad q_{3b} = 5.5$$

Solution: After substitution of the given numerical values, Eqs. (10.14a) and (10.16c) become, with c_i and s_i standing for $\cos\phi_i$ and $\sin\phi_i$, respectively,

$$\begin{aligned}
\mathcal{C}_1: \quad & 61.848 - 36.9561c_1 - 47.2376c_2 + 33.603c_1c_2 - 41.6822s_1s_2 = 0 \\
\mathcal{C}_2: \quad & -28.5721 + 48.6506c_1 - 20.7097c_1^2 + 68.7942c_2 - 100.811c_1c_2 \\
& +35.9634c_1^2c_2 - 41.4096c_2^2 + 50.8539c_1c_2^2 - 15.613c_1^2c_2^2 - 52.9789s_1^2 \\
& +67.6522c_2s_1^2 - 13.2765c_2^2s_1^2 + 74.1623s_1s_2 - 25.6617c_1s_1s_2 \\
& -67.953c_2s_1s_2 + 33.9241c_1c_2s_1s_2 - 13.202s_2^2 \\
& -3.75189c_1s_2^2 + 6.13542c_1^2s_2^2 = 0
\end{aligned}$$

The foregoing equations determine contours $\mathcal{C}_1$ and $\mathcal{C}_2$ in the ϕ_1–ϕ_2 plane, which are plotted in Fig. 10.7. Four real solutions are found by superimposing $\mathcal{C}_1$ and $\mathcal{C}_2$, as shown in this figure. The numerical values of the solutions, listed in Table 10.2, agree with the published results. Solutions 1 and 2 represent two poses of the

Table 10.2 Solutions for Nanua et al.'s example

No.	ϕ_1 (rad)	ϕ_2 (rad)	ϕ_3 (rad)
1	0.8335	0.5399	0.8528
2	1.5344	0.5107	0.2712
3	−0.8335	−0.5399	−0.8528
4	−1.5344	−0.5107	−0.2712

triangular plate over the base, while solutions 3 and 4 are just the reflections of solutions 1 and 2 with respect to the plane of the base plate. Hence, the geometric symmetry gives rise to an algebraic symmetry of the solutions.

Example 10.2.2 (The Univariate Polynomial Approach). Reduce the two equations found in Example 10.2.1, Eqs. (10.14a) and (10.16c), to a single monovariate polynomial equation.

Solution: We first substitute the trigonometric identities relating $c\phi_i$ and $s\phi_i$ with $\tau_i \equiv \tan(\phi_i/2)$, for $i = 1, 2$, into Eqs. (10.14a) and (10.16c). Upon clearing the denominators by multiplying those equations by $(1+\tau_1^2)(1+\tau_2^2)$, we obtain two polynomial equations in τ_1, namely,

$$G_1\tau_1^4 + G_2\tau_1^3 + G_3\tau_1^2 + G_4\tau_1 + G_5 = 0 \tag{10.17}$$

$$H_1\tau_1^2 + H_2\tau_1 + H_3 = 0 \tag{10.18}$$

where

$$\begin{aligned} G_1 &= K_1\tau_2^4 + K_2\tau_2^2 + K_3 \\ G_2 &= K_4\tau_2^3 + K_5\tau_2 \\ G_3 &= K_6\tau_2^4 + K_7\tau_2^2 + K_8 \\ G_4 &= K_9\tau_2^3 + K_{10}\tau_2 \\ G_5 &= K_{11}\tau_2^4 + K_{12}\tau_2^2 + K_{13} \end{aligned}$$

and

$$\begin{aligned} H_1 &= L_1\tau_2^2 + L_2 \\ H_2 &= L_3\tau_2 \\ H_3 &= L_4\tau_2^2 + L_5 \end{aligned}$$

In the above relations, $\{K_i\}_1^{13}$ and $\{L_i\}_1^5$ are all functions of the data. We now eliminate τ_1 from Eqs. (10.17) and (10.18), following Bezout's method, as given in (Salmon 1964). To do this, we multiply Eq. (10.17) by H_1 and Eq. (10.18) by $G_1\tau_1^2$, and subtract the two equations thus resulting, which leads to a cubic equation in τ_1, namely,

$$(G_2H_1 - G_1H_2)\tau_1^3 + (G_3H_1 - G_1H_3)\tau_1^2 + G_4H_1\tau_1 + G_5H_1 = 0 \tag{10.19a}$$

Likewise, if Eq. (10.17) is multiplied by $H_1\tau_1 + H_2$ and Eq. (10.18) by $G_1\tau_1^3 + G_2\tau_1^2$ and the equations thus resulting are subtracted from each other, one more cubic equation in τ_1 is obtained, namely,

$$(G_1H_3 - G_3H_1)\tau_1^3 + (G_4H_1 + G_3H_2 - G_2H_3)\tau_1^2 + (G_5H_1 + G_4H_2)\tau_1 + G_5H_2 = 0 \tag{10.19b}$$

Moreover, if we multiply Eq. (10.18) by τ_1, a third cubic equation in τ_1 can be derived, i.e.,

$$H_1\tau_1^3 + H_2\tau_1^2 + H_3\tau_1 = 0 \tag{10.19c}$$

Now, Eqs. (10.18) and (10.19a–c) constitute a homogeneous linear system of four equations in the first four powers of τ_1, which can be cast in the form

$$\mathbf{H}\boldsymbol{\tau}_1 = \mathbf{0} \tag{10.20}$$

where $\boldsymbol{\tau}_1 \equiv \left[\tau_1^3 \;\; \tau_1^2 \;\; \tau_1 \;\; 1\right]^T$ and

$$\mathbf{H} \equiv \begin{bmatrix} G_2H_1 - G_1H_2 & G_3H_1 - G_1H_3 & G_4H_1 & G_5H_1 \\ G_3H_1 - G_1H_3 & G_3H_2 - G_2H_3 + G_4H_1 & G_4H_2 + G_5H_1 & G_5H_2 \\ H_1 & H_2 & H_3 & 0 \\ 0 & H_1 & H_2 & H_3 \end{bmatrix}$$

In order for Eq. (10.20) to admit a nontrivial solution, the determinant of its coefficient matrix must vanish, i.e.,

$$\det(\mathbf{H}) = 0 \tag{10.21}$$

Given the definitions of $\{G_k\}_1^5$ and $\{H_k\}_1^3$, it is apparent that G_1, G_3, and G_5 are quartic, while G_2 and G_4 are cubic polynomials in τ_2. Likewise, H_1 and H_3 are quadratic, while H_2 is linear in τ_2 as well. As a result, the highest-degree entries of the first and second rows of $\mathbf{H}$ are sextic, while those of its third and fourth rows are quadratic. The outcome is that $\det(\mathbf{H})$ is of degree $6+6+2+2 = 16$, i.e., $\det(\mathbf{H})$ is a 16th-degree polynomial in τ_2. This equation, in general, admits up to 16 different solutions. Furthermore, the roots of the polynomial appear in the form of either complex conjugate pairs or real pairs. In the latter case, each pair represents two symmetric positions of the mobile platform with respect to the base, i.e., for each solution found above the base, another, mirror-imaged, solution exists below it. This symmetry exists, in general, as long as the six base attachment points are coplanar.

Other parallel manipulators are the planar and spherical counterparts of that studied above, and sketched in Figs. 10.8 and 10.9. The direct kinematics of the manipulator of Fig. 10.8 was found to admit up to six real solutions (Gosselin et al. 1992),

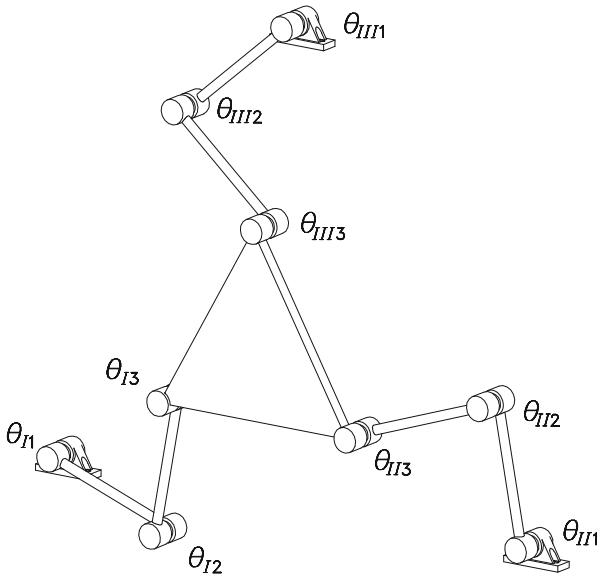

Fig. 10.8 A planar parallel manipulator

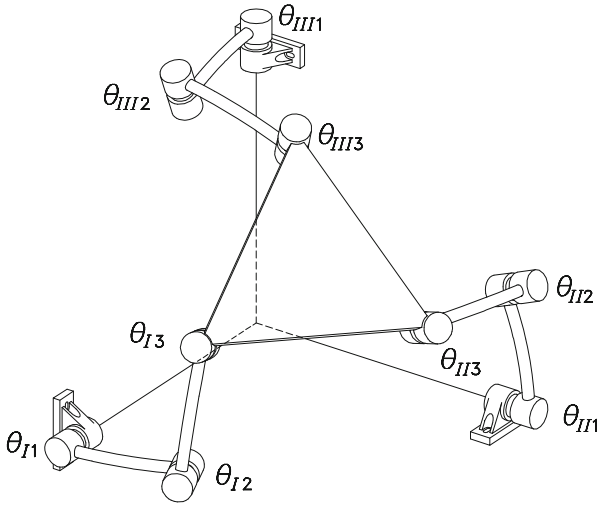

Fig. 10.9 A spherical parallel manipulator

while the spherical manipulator of Fig. 10.9 has been found to admit up to eight direct kinematic solutions (Gosselin et al. 1994a,b). A comprehensive account of the simulation and design of three-dof spherical parallel manipulators, which includes workspace analysis as well, is included in (Gosselin et al. 1995).

10.2.1 Velocity and Acceleration Analyses of Parallel Manipulators

Now we proceed to the velocity analysis of the manipulator of Fig. 10.2a. The inverse velocity analysis of this manipulator consists in determining the six rates of the active joints, $\{\dot{b}_k\}_1^6$, given the twist $\mathbf{t}$ of the moving platform. The velocity analysis of a typical leg leads to a relation of the form of Eq. (5.9), namely,

$$\mathbf{J}_J \dot{\boldsymbol{\theta}}_J = \mathbf{t}_J, \quad J = I, II, \ldots, VI \tag{10.22a}$$

where $\mathbf{J}_J$ is the Jacobian of the Jth leg, $\dot{\boldsymbol{\theta}}_J$ is the six-dimensional joint-rate vector of the same leg, and $\mathbf{t}_J$ is the twist of the moving platform $\mathcal{M}$, with its operation point defined as the point C_J of concurrency of the three revolutes composing the spherical joint of attachment of the leg to the moving platform $\mathcal{M}$, and shown in Fig. 10.3 as C, subscript J indicating that point C of that figure is different for different legs. We thus have

$$\mathbf{J}_J \equiv \begin{bmatrix} \mathbf{e}_1 & \mathbf{e}_2 & \mathbf{0} & \mathbf{e}_4 & \mathbf{e}_5 & \mathbf{e}_6 \\ b_{34}\mathbf{e}_1 \times \mathbf{e}_3 & b_{34}\mathbf{e}_2 \times \mathbf{e}_3 & \mathbf{e}_3 & \mathbf{0} & \mathbf{0} & \mathbf{0} \end{bmatrix}_J \tag{10.22b}$$

$$\mathbf{t}_J = \begin{bmatrix} \boldsymbol{\omega} \\ \dot{\mathbf{c}}_J \end{bmatrix}, \quad b_{34} \equiv b_3 + b_4 \tag{10.22c}$$

where the leg geometry has been taken into account.

Furthermore, from Fig. 10.3, it is apparent that

$$\dot{\mathbf{c}}_J = \dot{\mathbf{p}} - \boldsymbol{\omega} \times \mathbf{r}_J \tag{10.23}$$

with $\mathbf{r}_J$ defined as the vector directed from C_J to the operation point P of the moving platform.

Now, we regard the axes of the five revolute joints of the six-joint leg of Fig. 10.3 as a set of five zero-pitch screws $\mathcal{S} = \{\mathbf{s}_1, \mathbf{s}_2, \mathbf{s}_4, \mathbf{s}_5, \mathbf{s}_6\}$. The line passing through O_1 and C is a zero-pitch screw $\mathbf{s}_3$ reciprocal to $\mathcal{S}$, as shown below:

Since $\mathbf{s}_3$ passes through O_1, its moment with respect to this point vanishes, and hence,

$$\mathbf{s}_3 = \begin{bmatrix} \mathbf{e}_3 \\ \mathbf{0} \end{bmatrix}$$

Now it is simple matter to show that

$$\mathbf{s}_3^T \boldsymbol{\Gamma} \mathbf{s}_k = (\boldsymbol{\Gamma} \mathbf{s}_3)^T \mathbf{s}_k = 0 \quad \text{for} \quad k = 1, 2, 4, 5, 6 \tag{10.24}$$

and $\boldsymbol{\Gamma}$ given in Eq. (3.112), q.e.d.

Notice that, for the Jth leg,

$$\mathbf{\Gamma}\mathbf{s}_3 = \begin{bmatrix} \mathbf{0} \\ \mathbf{e}_3 \end{bmatrix}_J \equiv \mathbf{l}_J$$

and hence, on the one hand,

$$\mathbf{l}_J^T \mathbf{J}_J \dot{\boldsymbol{\theta}}_J = (\dot{b}_3)_J$$

where the subscript J reminds us that $\dot{b}_3$ is different for each leg. In order to ease the notation, and since we have a single variable b_3 per leg, we define henceforth

$$b_J \equiv (b_3)_J \tag{10.25a}$$

and hence, the above relation between $\mathbf{t}_J$ and the actuated joint rate of the Jth leg takes the form

$$\mathbf{l}_J^T \mathbf{J}_J \dot{\boldsymbol{\theta}}_J = \dot{b}_J \tag{10.25b}$$

On the other hand,

$$\mathbf{l}_J^T \mathbf{t}_J = (\mathbf{e}_3^T)_J \dot{\mathbf{c}}_J$$

Likewise, we define

$$(\mathbf{e}_3)_J \equiv \mathbf{e}_J \tag{10.26a}$$

the foregoing relation thus yielding

$$\mathbf{l}_J^T \mathbf{t}_J \equiv \mathbf{e}_J^T \dot{\mathbf{c}}_J \tag{10.26b}$$

Note that vectors $\mathbf{e}_J$ and $\mathbf{r}_J$ define uniquely the line along the two attachment points of the Jth leg. Henceforth, this line will be termed the axis of the Jth leg.

Upon equating the right-hand sides of Eqs. (10.25b) and (10.26b), the desired expression for the actuated joint rate is derived, namely,

$$\dot{b}_J = \mathbf{e}_J^T \dot{\mathbf{c}}_J, \quad J = I, II, \ldots, VI \tag{10.27a}$$

That is, the Jth joint rate is nothing but the projection onto the Jth leg axis of the velocity of point C_J. Furthermore, upon substituting Eq. (10.23) into Eq. (10.27a) above, we obtain the relations between the actuated joint rates and the twist of the moving platform, namely,

$$\dot{b}_J = \begin{bmatrix} (\mathbf{e}_J \times \mathbf{r}_J)^T & \mathbf{e}_J^T \end{bmatrix} \begin{bmatrix} \boldsymbol{\omega} \\ \dot{\mathbf{p}} \end{bmatrix} \equiv \mathbf{k}_J^T \mathbf{t} \tag{10.27b}$$

for $J = I, II, \ldots, VI$. Upon assembling all six leg-equations of Eq. (10.27b), we obtain the desired relation between the vector of actuated joint rates and the twist of the moving platform, namely,

$$\dot{\mathbf{b}} = \mathbf{K}\mathbf{t} \tag{10.28a}$$

with the six-dimensional vectors $\mathbf{b}$ and $\mathbf{t}$ defined as the vector of joint variables and the twist of the platform at the operation point, respectively. Moreover, the 6×6 matrix $\mathbf{K}$ is the Jacobian of the manipulator at hand. These quantities are displayed below:

$$\mathbf{b} \equiv \begin{bmatrix} b_I \\ b_{II} \\ \vdots \\ b_{VI} \end{bmatrix}, \quad \mathbf{t} \equiv \begin{bmatrix} \boldsymbol{\omega} \\ \dot{\mathbf{p}} \end{bmatrix}, \quad \mathbf{K} \equiv \begin{bmatrix} (\mathbf{e}_I \times \mathbf{r}_I)^T & \mathbf{e}_I^T \\ (\mathbf{e}_{II} \times \mathbf{r}_{II})^T & \mathbf{e}_{II}^T \\ \vdots & \\ (\mathbf{e}_{VI} \times \mathbf{r}_{VI})^T & \mathbf{e}_{VI}^T \end{bmatrix} \tag{10.28b}$$

From the above display, it is apparent that each row of $\mathbf{K}$ is the transpose of the Plücker array of the corresponding leg axis, although in axis coordinates, as opposed to the Jacobian matrix $\mathbf{J}$ of serial manipulators, whose columns are the Plücker coordinates of the corresponding joint axis in ray coordinates. Moreover, in these coordinates, the moment of the leg-axis is taken with respect to the operation point P of $\mathcal{M}$. One more difference between the velocity analysis of serial and parallel manipulators is the role played by the actuator joint rates in the underlying forward and direct kinematics. In the case of parallel manipulators, this role is changed, for now we have that the actuator joint rates are given by explicit formulas in terms of the twist of the moving platform, along with the manipulator architecture and configuration. Finding the platform twist requires inverting matrix $\mathbf{K}$. Moreover, the significance of singularities also changes: When $\mathbf{K}$ becomes singular, some instantaneous motions of the platform are possible even if all actuated joints are kept locked. That is, a singularity of $\mathbf{K}$ is to be interpreted now as the inability of the manipulator to withstand a certain static wrench. An extensive analysis of the singularities of parallel manipulators using line geometry in a form that is known as *Grassmann geometry* was reported by Merlet (1989).

Now, the acceleration analysis of the same leg is straightforward. Indeed, upon differentiation of both sides of Eq. (10.28a) with respect to time, one obtains

$$\ddot{\mathbf{b}} = \mathbf{K}\dot{\mathbf{t}} + \dot{\mathbf{K}}\mathbf{t} \tag{10.29a}$$

where $\dot{\mathbf{K}}$ takes the form

$$\dot{\mathbf{K}} = \begin{bmatrix} \dot{\mathbf{u}}_I^T & \dot{\mathbf{e}}_I^T \\ \dot{\mathbf{u}}_{II}^T & \dot{\mathbf{e}}_I^T \\ \vdots & \\ \dot{\mathbf{u}}_{VI}^T & \dot{\mathbf{e}}_{VI}^T \end{bmatrix} \tag{10.29b}$$

and $\mathbf{u}_J$ is defined as

$$\mathbf{u}_J \equiv \mathbf{e}_J \times \mathbf{r}_J \tag{10.29c}$$

Therefore,

$$\dot{\mathbf{u}}_J = \dot{\mathbf{e}}_J \times \mathbf{r}_J + \mathbf{e}_J \times \dot{\mathbf{r}}_J \tag{10.29d}$$

Now, since vectors $\mathbf{r}_J$ are fixed to the moving platform, their time-derivatives are simply given by

$$\dot{\mathbf{r}}_J = \boldsymbol{\omega} \times \mathbf{r}_J \tag{10.29e}$$

On the other hand, vector $\mathbf{e}_J$ is directed along the leg axis, and so, its time-derivative is given by

$$\dot{\mathbf{e}}_J = \boldsymbol{\omega}_J \times \mathbf{e}_J$$

with $\boldsymbol{\omega}_J$ defined as the angular velocity of the third leg link, i.e.,

$$\boldsymbol{\omega}_J = (\dot{\theta}_1 \mathbf{e}_1 + \dot{\theta}_2 \mathbf{e}_2)_J$$

the subscript J of the above parentheses reminding us that this angular velocity differs from leg to leg. Clearly, we need expressions for the rates of the first two joints of each leg. Below we derive the corresponding expressions. In order to simplify the notation, we start by defining

$$\mathbf{f}_J \equiv (\mathbf{e}_1)_J, \quad \mathbf{g}_J \equiv (\mathbf{e}_2)_J \tag{10.29f}$$

Now we write the second vector equation of Eq. (10.22a) using the foregoing definitions, which yields

$$(\dot{\theta}_1)_J \mathbf{f}_J \times (b_J + b_4)\mathbf{e}_J + (\dot{\theta}_2)_J \mathbf{g}_J \times (b_J + b_4)\mathbf{e}_J + \dot{b}_J \mathbf{e}_J = \dot{\mathbf{c}}_J$$

where b_4 is the same for all legs, since all have identical architectures. Now we can eliminate $(\dot{\theta}_2)_J$ from the foregoing equation by dot-multiplying its two sides by $\mathbf{g}_J$, thereby producing

$$(\dot{\theta}_1)_J \mathbf{g}_J \times \mathbf{f}_J \cdot (b_J + b_4)\mathbf{e}_J + \mathbf{g}_J^T (\mathbf{e}_J \mathbf{e}_J^T)\dot{\mathbf{c}}_J = \mathbf{g}^T \dot{\mathbf{c}}_J$$

where an obvious exchange of the cross and the dot in the above equation has taken place, and expression (10.27a) for $\dot{b}_J$ has been recalled. Now it is a simple matter to solve for $(\dot{\theta}_1)_J$ from the above equation, which yields

$$(\dot{\theta}_1)_J = -\frac{\mathbf{g}_J^T (\mathbf{1} - \mathbf{e}_J \mathbf{e}_J^T)\dot{\mathbf{c}}_J}{\Delta_J}$$

with Δ_J defined as

$$\Delta_J \equiv (b_J + b_4)\mathbf{e}_J \times \mathbf{f}_J \cdot \mathbf{g}_J \tag{10.30}$$

Moreover, we can obtain the above expression for $(\dot{\theta}_1)_J$ in terms of the platform twist by recalling Eq. (10.23), which is reproduced below in a more suitable form for quick reference:

$$\dot{\mathbf{c}}_J = \mathbf{C}_J \mathbf{t}$$

where $\mathbf{t}$ is the twist of the platform, the 3×6 matrix $\mathbf{C}_J$ being defined as

$$\mathbf{C}_J \equiv \begin{bmatrix} \mathbf{R}_J & \mathbf{1} \end{bmatrix}$$

in which $\mathbf{R}_J$ is the cross-product matrix of $\mathbf{r}_J$ and $\mathbf{1}$ is the 3×3 identity matrix. Therefore, the expression sought for $(\dot{\theta}_1)_J$ takes the form

$$(\dot{\theta}_1)_J = -\frac{1}{\Delta_J}\mathbf{g}_J^T(\mathbf{1} - \mathbf{e}_J\mathbf{e}_J^T)\mathbf{C}_J\mathbf{t}, \quad J = I, II, \ldots, VI \tag{10.31a}$$

A similar procedure can be followed to find $(\dot{\theta}_2)_J$, the final result being

$$(\dot{\theta}_2)_J = \frac{1}{\Delta_J}\mathbf{f}_J^T(\mathbf{1} - \mathbf{e}_J\mathbf{e}_J^T)\mathbf{C}_J\mathbf{t}, \quad J = I, II, \ldots, VI \tag{10.31b}$$

thereby completing the calculations required to obtain the rates of all unactuated joints. Note that the unit vectors involved in those calculations, $\mathbf{e}_J$, $\mathbf{f}_J$, and $\mathbf{g}_J$, are computed from the leg inverse kinematics, as discussed above.

Planar and Spherical Manipulators

The velocity analysis of the planar and spherical parallel manipulators of Figs. 10.8 and 10.9 are outlined below: Using the results of Sect. 5.7.2, the velocity relations of the Jth leg of the planar manipulator take the form

$$\mathbf{J}_J\dot{\boldsymbol{\theta}}_J = \mathbf{t}, \quad J = I, II, III \tag{10.32}$$

where $\mathbf{J}_J$ is the Jacobian matrix of this leg, as given by Eq. (5.60), while $\dot{\boldsymbol{\theta}}_J$ is the three-dimensional vector of joint rates of this leg, i.e.,

$$\mathbf{J}_J \equiv \begin{bmatrix} 1 & 1 & 1 \\ \mathbf{Er}_{J1} & \mathbf{Er}_{J2} & \mathbf{Er}_{J3} \end{bmatrix}, \quad \dot{\boldsymbol{\theta}}_J \equiv \begin{bmatrix} \dot{\theta}_{J1} \\ \dot{\theta}_{J2} \\ \dot{\theta}_{J3} \end{bmatrix}, \quad J = I, II, III$$

For purposes of kinematic velocity control, however, we are interested only in the first joint rate of each leg; i.e., all we need to determine in order to produce a desired twist of the end-effector is not all of the foregoing nine joint rates, but only $\dot{\theta}_{I1}$, $\dot{\theta}_{II1}$, and $\dot{\theta}_{III1}$. Thus, we want to eliminate from Eq. (10.32) the unactuated joint rates $\dot{\theta}_{J2}$ and $\dot{\theta}_{J3}$, which can be readily done if we multiply both sides of the said equation by a three-dimensional vector $\mathbf{n}_J$ perpendicular to the second and the third columns of $\mathbf{J}_J$. This vector can be most easily determined as the cross product of those two columns, namely, as

$$\mathbf{n} \equiv \mathbf{j}_{J2} \times \mathbf{j}_{J3} = \begin{bmatrix} -\mathbf{r}_{J2}^T \mathbf{E} \mathbf{r}_{J3} \\ \mathbf{r}_{J2} - \mathbf{r}_{J3} \end{bmatrix}$$

Upon multiplication of both sides of Eq. (10.32) by $\mathbf{n}_J^T$, we obtain

$$\left[-\mathbf{r}_{J2}^T \mathbf{E} \mathbf{r}_{J3} + (\mathbf{r}_{J2} - \mathbf{r}_{J3})^T \mathbf{E} \mathbf{r}_{J1} \right] \dot{\theta}_{J1} = -(\mathbf{r}_{J2}^T \mathbf{E} \mathbf{r}_{J3}) \omega + (\mathbf{r}_{J2} - \mathbf{r}_{J3})^T \dot{\mathbf{c}} \quad (10.33)$$

and hence, we can solve directly for $\dot{\theta}_{J1}$ from the foregoing equation, thereby deriving

$$\dot{\theta}_{J1} = \frac{-(\mathbf{r}_{J2}^T \mathbf{E} \mathbf{r}_{J3}) \omega + (\mathbf{r}_{J2} - \mathbf{r}_{J3})^T \dot{\mathbf{c}}}{-\mathbf{r}_{J2}^T \mathbf{E} \mathbf{r}_{J3} + (\mathbf{r}_{J2} - \mathbf{r}_{J3})^T \mathbf{E} \mathbf{r}_{J1}} \quad (10.34a)$$

Note that Eq. (10.33) can be written in the form

$$j_J \dot{\theta}_{J1} = \mathbf{k}_J^T \mathbf{t}, \quad J = I, II, III \quad (10.34b)$$

with j_J and $\mathbf{k}_J$ defined, for $J = I, II, III$, as

$$j_J \equiv (\mathbf{r}_{J2} - \mathbf{r}_{J3})^T \mathbf{E} \mathbf{r}_{J1} - \mathbf{r}_{J2}^T \mathbf{E} \mathbf{r}_{J3},$$
$$\mathbf{k}_J \equiv \left[\mathbf{r}_{J2}^T \mathbf{E} \mathbf{r}_{J3} \; -(\mathbf{r}_{J2} - \mathbf{r}_{J3})^T \right]^T$$

If we further define

$$\dot{\boldsymbol{\theta}} \equiv \left[\dot{\theta}_{I1} \; \dot{\theta}_{II2} \; \dot{\theta}_{III3} \right]^T$$

and assemble all three foregoing joint-rate-twist relations, we obtain

$$\mathbf{J} \dot{\boldsymbol{\theta}} = \mathbf{K} \mathbf{t} \quad (10.35)$$

where $\mathbf{J}$ and $\mathbf{K}$ are the two manipulator Jacobians defined as

$$\mathbf{J} \equiv \mathrm{diag}(j_I, \; j_{II}, \; j_{III}), \quad \mathbf{K} \equiv \begin{bmatrix} \mathbf{k}_I^T \\ \mathbf{k}_{II}^T \\ \mathbf{k}_{III}^T \end{bmatrix} \quad (10.36)$$

Expressions for the joint accelerations can be readily derived by differentiation of the foregoing expressions with respect to time.

The velocity analysis of the spherical parallel manipulator of Fig. 10.9 can be accomplished similarly. Thus, the velocity relations of the Jth leg take on the form

$$\mathbf{J}_J \dot{\boldsymbol{\theta}}_J = \boldsymbol{\omega}, \quad J = I, II, III \tag{10.37}$$

where the Jacobian of the Jth leg, $\mathbf{J}_J$, is defined as

$$\mathbf{J}_J \equiv \left[\mathbf{e}_{J1}\ \mathbf{e}_{J2}\ \mathbf{e}_{J3}\right]$$

while the joint-rate vector of the Jth leg, $\dot{\boldsymbol{\theta}}_J$, is defined exactly as in the planar case analyzed above. Again, for kinematic velocity control purposes, we are interested only in the actuated joint rates, namely, $\dot{\theta}_{I1}$, $\dot{\theta}_{II1}$, and $\dot{\theta}_{III1}$. As in the planar case, we can eliminate $\dot{\theta}_{J2}$ and $\dot{\theta}_{J3}$ upon multiplication of both sides of Eq. (10.37) by a vector $\mathbf{n}_J$ perpendicular to the second and the third columns of $\mathbf{J}_J$. An obvious definition of this vector is, then,

$$\mathbf{n}_J \equiv \mathbf{e}_{J2} \times \mathbf{e}_{J3}$$

The desired joint-rate relation is thus readily derived as

$$j_J \dot{\theta}_{J1} = \mathbf{k}_J^T \boldsymbol{\omega}, \quad J = I, II, III \tag{10.38}$$

where j_J and $\mathbf{k}_J$ are now defined as

$$j_J \equiv \mathbf{e}_{J1} \times \mathbf{e}_{J2} \cdot \mathbf{e}_{J3} \tag{10.39a}$$

$$\mathbf{k}_J \equiv \mathbf{e}_{J2} \times \mathbf{e}_{J3} \tag{10.39b}$$

The accelerations of the actuated joints can be derived, again, by differentiation of the foregoing expressions.

We can then say that in general, parallel manipulators, as opposed to serial ones, *have two Jacobian matrices*.

10.3 Multifingered Hands

Shown in Fig. 10.10 is a three-fingered hand with fingers $\mathcal{A}$, $\mathcal{B}$, and $\mathcal{C}$, each supplied with three revolute joints. Furthermore, each finger carries two revolutes of parallel axes that are normal to the axis of the third one. Thus, each finger comprises three links, the one closest to the palm $\mathcal{P}$ being of virtually zero length and coupled to $\mathcal{P}$ via a revolute joint. Of the other two, that in contact with the object $\mathcal{O}$ is the *distal phalanx*, the other being the *proximal phalanx*. Moreover, the fingers can be either *hard* or *soft*; if the latter, then contact takes place over a finite area; if the former, then contact takes place over a point, and hence, hard fingers can exert only force and no

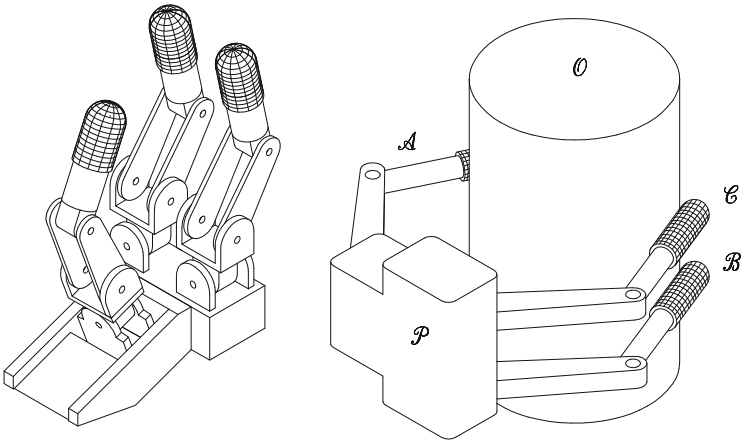

Fig. 10.10 A three-fingered hand

moment on the manipulated object. Soft fingers can exert both force and moment. For the sake of conciseness, we will deal only with hard fingers here. Let the contact points of fingers $\mathcal{A}$, $\mathcal{B}$, and $\mathcal{C}$ with $\mathcal{O}$ be denoted by A_O, B_O, and C_O, respectively. The purpose of the hand is to manipulate $\mathcal{O}$ with respect to $\mathcal{P}$. The motion of $\mathcal{O}$, moreover, can be specified through its pose, given in turn by the position vector $\mathbf{o}$ of one of its points, O, and its orientation matrix $\mathbf{Q}$ with respect to a frame fixed to $\mathcal{P}$. Now, in order to manipulate $\mathcal{O}$ six degrees of freedom are needed. When the three fingers are in contact with $\mathcal{O}$, the hand-object system forms a parallel manipulator with three "legs" of the RRS type, with S standing for spherical joint. As the reader can verify, the system has six-dof, which means that manipulations are possible with only two actuated revolutes per finger. Many designs involve only two motors per finger, one of the revolute joints being provided with springs to guarantee contact.

Thus, the location of the three contact points is fully determined if the pose of $\mathcal{P}$ and the locations of A_O, B_O, and C_O in $\mathcal{O}$ are given. Once the position vectors of the three contact points are known, determining the joint-variable values needed to take $\mathcal{O}$ to the desired pose reduces to solving a three-dimensional positioning problem for each finger, with three revolute joints—a problem already discussed in Sect. 4.4.1. The joint rates and accelerations are then determined as in Sects. 4.4 and 5.5.

While the mechanics of grasping is quite elaborate, due to the deformation of both fingers and object, some assumptions will be introduced here to produce a simple model. One such assumption is rigidity; a second is *smoothness*, under which each finger is capable of exerting only normal force on the object. Moreover, this force is *unidirectional*, for the finger cannot exert a *pull* on the object. The smoothness and rigidity assumptions bring about limitations, for they require a rather large number of fingers to exert an arbitrary wrench on the grasped object, as shown below.

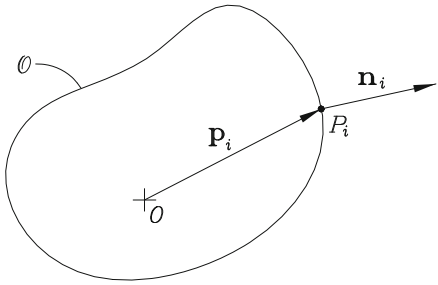

Fig. 10.11 Geometry of grasped object $\mathcal{O}$

We assume that we have a rigid object $\mathcal{O}$ bounded by a surface $\mathcal{S}$ that is smooth *almost everywhere*, i.e., it has a well-defined normal $\mathbf{n}$ everywhere except at either isolated points or isolated curves on $\mathcal{S}$. Below we show that in order to exert an arbitrary wrench $\mathbf{w}$ onto $\mathcal{O}$, a hand with rigid, smooth fingers should have more than six fingers. Assume that the n contact points on $\mathcal{S}$ are $\{P_i\}_1^n$ and that we want to find n pressure values $\{\lambda_i\}_1^n$ at the contact points that will produce the desired wrench $\mathbf{w}$ onto $\mathcal{O}$.

Moreover, let the unit normal at P_i be denoted by $\mathbf{n}_i$ and the vector directed from O to P_i be denoted by $\mathbf{p}_i$, as shown in Fig. 10.11.

The wrench $\mathbf{w}_i$ exerted by each finger onto $\mathcal{O}$ at P_i is apparently

$$\mathbf{w}_i = \lambda_i \begin{bmatrix} \mathbf{p}_i \times (-\mathbf{n}_i) \\ -\mathbf{n}_i \end{bmatrix}, \quad \lambda_i \geq 0$$

Upon equating the resultant wrench with the desired wrench, we obtain

$$\sum_1^n \begin{bmatrix} -\mathbf{p}_i \times \mathbf{n}_i \\ -\mathbf{n}_i \end{bmatrix} \lambda_i = \mathbf{w}$$

or in compact form, as

$$\mathbf{G}\boldsymbol{\lambda} = -\mathbf{w} \tag{10.40a}$$

where $\mathbf{G}$ is the $6 \times n$ *grasping matrix* and $\boldsymbol{\lambda}$ is the n-dimensional vector of pressure values, i.e.,

$$\mathbf{G} \equiv \begin{bmatrix} \mathbf{p}_1 \times \mathbf{n}_1 & \cdots & \mathbf{p}_n \times \mathbf{n}_n \\ \mathbf{n}_1 & \cdots & \mathbf{n}_n \end{bmatrix}, \qquad \boldsymbol{\lambda} \equiv \begin{bmatrix} \lambda_1 \\ \vdots \\ \lambda_n \end{bmatrix} \tag{10.40b}$$

Note that the ith column of the grasping matrix is nothing but the array of Plücker coordinates of the line of action of the force exerted by the ith finger on the object, in ray coordinates—see Sect. 3.2.2.

Thus, for $n = 6$, a unique pressure vector $\boldsymbol{\lambda}$ is obtained as long as $\mathbf{G}$ is nonsingular. However, negative values of $\{\lambda_i\}_1^n$ are not allowed, and since nothing prevents these values from becoming negative, six fingers of the type considered here are not enough. We must thus have more than six such fingers in order to be able to apply an arbitrary wrench onto the body. For $n > 6$ and a full-rank $6 \times n$ grasping matrix, nonnegative values of $\{\lambda_i\}_1^n$ can be generated, but only under certain conditions, as explained below: Let $\mathbf{u}$ be a vector lying in the null space of $\mathbf{G}$, i.e., such that $\mathbf{Gu} = \mathbf{0}$. Then an arbitrary $\boldsymbol{\lambda}$ can be expressed as

$$\boldsymbol{\lambda} = \boldsymbol{\lambda}_0 + \mathbf{u}$$

where $\boldsymbol{\lambda}_0$ is a *particular solution* of Eq. (10.40a). For example, if $\boldsymbol{\lambda}_0$ is chosen as the *minimum-norm solution* of Eq. (10.40a), then we have, explicitly,

$$\boldsymbol{\lambda}_0 = -\mathbf{G}^{\dagger}\mathbf{w}$$

where $\mathbf{G}^{\dagger}$ is the *generalized inverse* of $\mathbf{G}$, defined as

$$\mathbf{G}^{\dagger} \equiv \mathbf{G}^T(\mathbf{G}\mathbf{G}^T)^{-1}$$

The numerical computation of the minimum norm solution of an undetermined system of linear equations is discussed in Appendix B.

Note that the 6×6 product $\mathbf{G}\mathbf{G}^T$ has the general form

$$\mathbf{G}\mathbf{G}^T = \begin{bmatrix} \sum_1^n (\mathbf{p}_i \times \mathbf{n}_i)(\mathbf{p}_i \times \mathbf{n}_i)^T & \sum_1^n (\mathbf{p}_i \times \mathbf{n}_i)\mathbf{n}_i^T \\ \sum_1^n \mathbf{n}_i (\mathbf{p}_i \times \mathbf{n}_i)^T & \mathbf{n}_i \mathbf{n}_i^T \end{bmatrix}$$

Although a symbolic expression for the inverse $\mathbf{H}$ of $\mathbf{G}\mathbf{G}^T$ is not possible in the general case, we can always express this inverse in block form, with all blocks of 3×3, namely,

$$\mathbf{H} \equiv (\mathbf{G}\mathbf{G}^T)^{-1} = \begin{bmatrix} \mathbf{H}_{11} & \mathbf{H}_{12} \\ \mathbf{H}_{12}^T & \mathbf{H}_{22} \end{bmatrix}$$

where consistently, $\mathbf{H}_{11}$ has units of meter^{-2}, $\mathbf{H}_{12}$ has units of meter^{-1}, and $\mathbf{H}_{22}$ is dimensionless. Moreover, we can partition $\mathbf{G}$ into two $3 \times n$ blocks, i.e.,

$$\mathbf{G} \equiv \begin{bmatrix} \mathbf{A} \\ \mathbf{B} \end{bmatrix}$$

in which $\mathbf{A}$ has units of meter, while $\mathbf{B}$ is dimensionless. Hence, the product $\mathbf{G}^T\mathbf{H}$ takes on the form

$$\mathbf{G}^T\mathbf{H} = \begin{bmatrix} \mathbf{A}^T\mathbf{H}_{11} + \mathbf{B}^T\mathbf{H}_{12}^T & \mathbf{A}^T\mathbf{H}_{12} + \mathbf{B}^T\mathbf{H}_{22} \end{bmatrix}$$

and hence, the left-hand block of the foregoing product has units of meter^{-1}, while the right-hand block is dimensionless. Upon multiplying the desired wrench $\mathbf{w}$ from the left by this product, the result, $\boldsymbol{\lambda}_0$, has consistently units of Newton.

Now, to find $\mathbf{u}$, several numerical methods are available that do not require any matrix inversion (Golub and Van Loan 1989). A simple way of expressing $\mathbf{u}$, although by no means the way to compute it, is given by

$$\mathbf{u} = \mathbf{P}\mathbf{v}, \quad \mathbf{P} \equiv \mathbf{1} - \mathbf{G}^{\dagger}\mathbf{G}$$

where $\mathbf{v}$ is an n-dimensional vector and $\mathbf{P}$ is a matrix *projecting* $\mathbf{v}$ onto the null space of $\mathbf{G}$, and $\mathbf{1}$ defined as the $n \times n$ identity matrix. Now we are left with the task of finding $\mathbf{v}$ so that

$$\lambda_i = \lambda_{0i} + u_i \geq 0, \quad i = 1, \ldots, n$$

Hence, our policy to determine $\mathbf{u}$ is simply, for $i = 1, \ldots, n$,

$$u_i = \begin{cases} 0, & \text{if } \lambda_{0i} \geq 0; \\ -\lambda_{0i}, & \text{otherwise.} \end{cases}$$

Further, $\mathbf{v}$ is found upon solving

$$\mathbf{P}\mathbf{v} = \mathbf{u}$$

However, $\mathbf{P}$ is singular—its rank is $n - 6$, as the reader is invited to prove—and the above equation may or may not admit a solution. For a solution to be possible, $\mathbf{u}$ must lie in the null space of $\mathbf{G}$.

A more general approach to solving the grasping problem relies on linear programming, but this topic lies beyond the scope of the book. The interested reader is directed to the specialized literature on the subject (Hillier and Lieberman 1995).

In the presence of soft fingers, however, fewer than six fingers suffice to grasp an object. Moreover, in the presence of friction, the force transmitted by a finger has, in addition to its normal component, a tangential component that, hence, gives rise to a contact force making a nonzero angle with the normal $\mathbf{n}_i$ to the object surface at the ith contact point. Therefore, by virtue of the linear relation between the normal and the tangential components of the transmitted force, given by the coefficient of friction μ, this force is constrained to lie within the *friction cone*. This cone has its apex at the contact point P_i, its elements making an angle α with the normal, that is given by $\alpha = \arctan(\mu)$. Furthermore, by virtue of the fundamental assumption of Coulomb friction analysis, μ lies between 0 and 1, and hence, α is constrained to lie between 0° and 45°.

Shown in Fig. 10.12 is an example of a three-fingered hand. This hand was developed at the Katholieke Universiteit Leuven (Van Brussel et al. 1989).

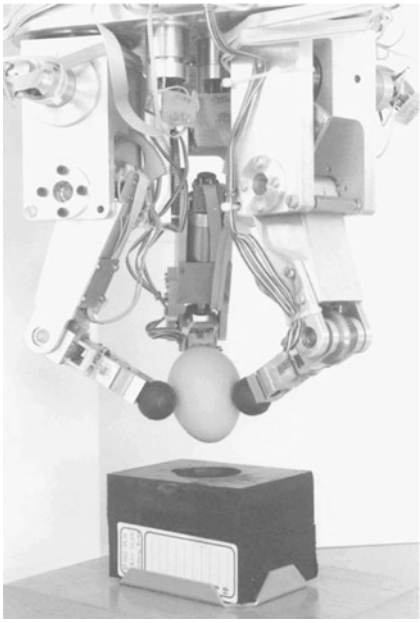

Fig. 10.12 A prototype of the KU Leuven three-fingered hand (courtesy of Prof. H. Van Brussel)

The literature on multifingered hands and the problem of grasping is far richer than we can afford to describe here. Extensive studies on these subjects have been reported by Reynaerts (1995) and Teichmann (1995).

10.4 Walking Machines

Besides the walking machines introduced in Chap. 1, namely, the OSU Adaptive Suspension Vehicle and the TUM Hexapod, other legged machines or leg designs are emerging with special features. For example, CARL, shown in Fig. 10.13, is a compliant articulated robot leg that was designed at McGill University's Centre for Intelligent Machines (CIM) by Prof. Buehler and his team (Menitto and Buehler 1996). This leg contains an actuation package with a high load-carrying capacity (ATLAS) and an antagonistic pair of concentric translational-to-angular displacement devices. The leg has four degrees of freedom, of which two are actuated by ATLAS and one by a harmonic drive motor, while one is unactuated. This leg design is intended to provide locomotion to a quadruped.

As nature shows in mammals, four legs are necessary to guarantee the static equilibrium of the body while one leg is in the swing phase. Static equilibrium is achieved as long as the horizontal projection of the mass center of the overall body-legs system lies within the triangle defined by the contact points of the three legs that are in the stance phase. More than four legs would allow for greater mobility. For purposes of symmetry, some walking machines are designed as hexapods, so as to allow for an equal number of legs in the swing and the stance phases.

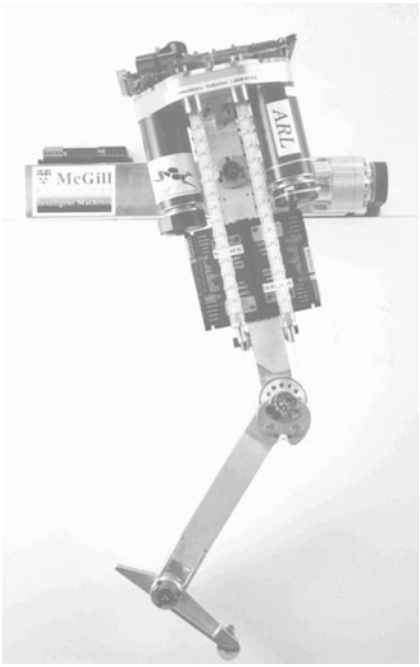

Fig. 10.13 The compliant articulated robot leg (courtesy of Prof. M. Buehler)

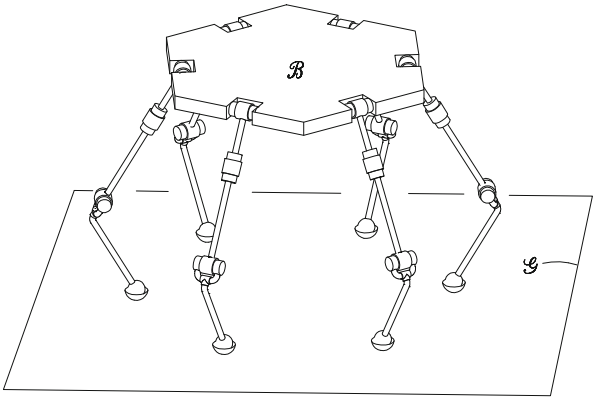

Fig. 10.14 A general hexapod

The kinematic analysis of walking machines is possible using the hexapod displayed in Fig. 10.14.

Furthermore, contact with the ground is assumed to take place such that the ground can exert only a "pushing" force on each leg but no moment. Thus, while we can model the contact between leg and ground as a spherical joint, care must be taken so that no pulls of the ground on the leg are required for a given gait.

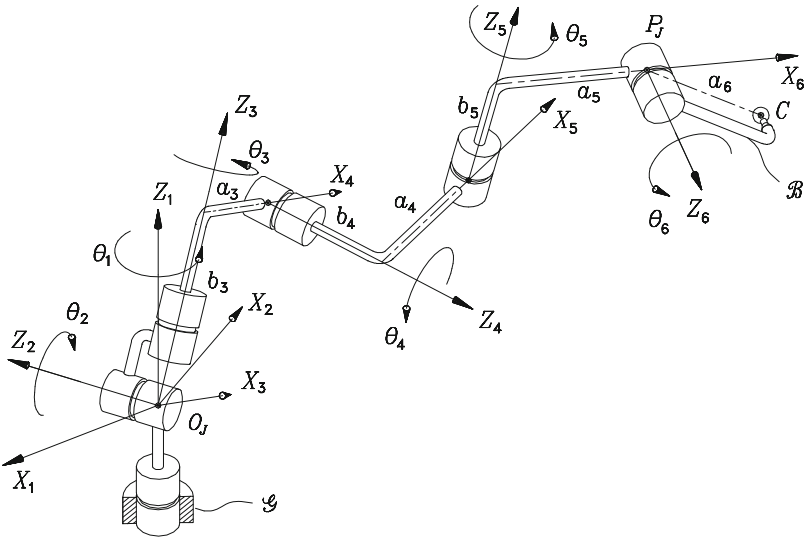

Fig. 10.15 One of the legs of a walking machine with three actuated revolutes

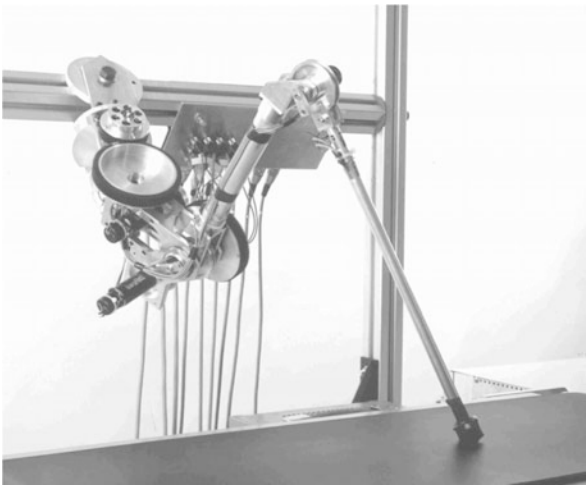

Fig. 10.16 One of the six identical legs of the TU Munich Hexapod (courtesy of Prof. F. Pfeiffer. Reproduced with permission of TSI Enterprises, Inc.)

Additionally, we shall assume that the leg is actuated by three revolutes, namely, those with variables θ_4, θ_5, and θ_6 in Fig. 10.15, where $\mathcal{G}$ denotes the ground and $\mathcal{B}$ the machine body. A photograph of one of the six identical legs of the walking machine developed at the Technical University of Munich, introduced in Fig. 1.11, is included in Fig. 10.16. The Denavit–Hartenberg parameters of this leg, proceeding from the ground upwards, are displayed in Table 10.3. Note that the architecture of this leg is simply that of a three-revolute manipulator carrying a spherical joint at its end-effector, similar to that of the decoupled manipulators studied in Sect. 4.4.

Table 10.3 DH parameters of the leg of the TU-Munich walking machine

i	a_i (mm)	b_i (mm)	α_i
1	17	0	90°
2	123	0	180°
3	116	0	0°
4	0	0	90°
5	0	0	90°
6	0	0	0°

The spherical joint accounts for the coupling of the leg with the ground. We are thus assuming that when a leg is in contact with the ground, the contact point of the leg is immobile. At the same time, the motion of the body $\mathcal{B}$ is prescribed through the motion of a point on the axis of the revolute coupled to the body. Such a point is indicated by P_J for the Jth leg. Moreover, the point of the Jth leg in contact with the ground will be denoted by O_J. Thus, when prescribing the motion of the body through that of each of the six points P_I, P_{II}, ..., P_{VI}, the rigid-body compatibility conditions of Eqs. (8.14), (8.15), and (8.28) must be observed. The pose of the body $\mathcal{B}$ is thus specified by the position of a point C of the body and the orientation matrix $\mathbf{Q}$ of the body with respect to a frame fixed to the ground, the position vector of C in that frame being denoted by $\mathbf{c}$. The specification of points P_I to P_{VI} thus follows from the knowledge of $\mathbf{c}$ and $\mathbf{Q}$, thereby guaranteeing compliance with the above-mentioned constraints.

Furthermore, a maneuver of $\mathcal{B}$, given by a prescribed pose, can be achieved by suitable values of the actuated-joint variables, which thus leads to a problem of parallel-manipulator inverse kinematics.

The mechanical system that results from the kinematic coupling of the machine legs with the ground is thus equivalent to a parallel manipulator. The essential difference between a walking machine and a parallel manipulator is that the former usually involves more actuators than degrees of freedom. This feature is known as *redundant actuation* and will not be pursued here.

10.5 Rolling Robots

Probably the rolling robot that has received most media attention is NASA's *Sojourner*, of the *Pathfinder* mission, which explored a spot of the Martian landscape for several months in 1997. It is noteworthy that the *Sojourner* was designed, built, and commissioned with a shoestring budget for NASA standards. The *Sojourner* is a paradigm of rolling robots for autonomous operation on rough terrain. We focus here on the simplest robots of this class, i.e., robots intended for tasks on horizontal surfaces, and so, their platforms undergo planar motion, which greatly simplifies their kinematics. One special feature of rolling robots is their *nonholonomic* nature. What this means is that the minimum number m of generalized coordinates defining uniquely a posture of the system is greater than

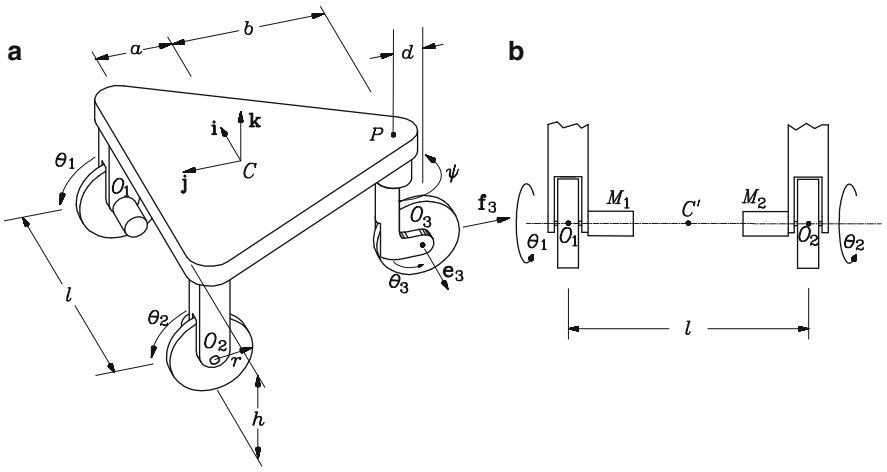

Fig. 10.17 A two-dof rolling robot: (**a**) its general layout; and (**b**) a detail of its actuated wheels

the number n of their independent generalized speeds, i.e., $m > n$. In the case of serial and parallel manipulators, paradigms of *holonomic* systems, $m = n$. In nonholonomic systems, then, we must distinguish between their posture, or configuration degree of freedom and their *mobility*, or velocity degree of freedom. For the sake of conciseness, we will refer to the latter whenever we mention the degree of freedom of a rolling robot.

Rolling robots are basically of two kinds, depending on whether they are supplied with conventional or with omnidirectional wheels. The simplest robots with conventional wheels are capable only of two-dof motions, and hence, are kinematically equivalent to conventional terrestrial vehicles. However, robots with omnidirectional wheels (ODWs) are capable of three-dof motions, which increases substantially their maneuverability. Below we outline the kinematics of the two kinds of robots.

10.5.1 Robots with Conventional Wheels

We begin with robots rolling on conventional wheels. Since these have two degrees of freedom, they need only two actuators, the various designs available varying essentially in where these actuators are located. The basic architecture of this kind of robot is displayed in Fig. 10.17a, in which we distinguish a chassis, or robot body, depicted as a triangular plate in that figure: two coaxial wheels that are coupled to the chassis by means of revolutes of axes passing through points O_1 and O_2; and a third wheel mounted on a bracket.

Now, the two actuators can be placed in two essentially different arrays. In the first array, not shown in the figure, one actuator is used for propulsion and the other for steering, the former being used to provide locomotion power to the common two-wheel axle via a differential gear train. This train is required to allow for different angular velocities of the two coaxial wheels. Moreover, the orientation of the mid-plane of the steering wheel, defined by angle ψ, is controlled with the second actuator. This design has some drawbacks, namely, (a) the two motors serving two essentially different tasks call for essentially different operational characteristics, to the point that both may not be available from the same manufacturer; (b) the propulsion motor calls for velocity control, the steering motor for position control, thereby giving rise to two independent control systems that may end up by operating in an uncoordinated fashion; and finally, (c) the use of a differential gear train increases cost, weight, and brings about the inherent backlash of gears.

In the second actuation array, shown in Fig. 10.17b, the two coaxial wheels are powered independently, thereby doing away with the differential train and its undesirable side effects, the third wheel being an idle caster. Moreover, the orientation of the latter is determined by friction and constraint forces, thereby making unnecessary the steering control system of the first array. Below we analyze the kinematics of a robot with this form of actuation.

Let point C of the platform be the *operation point*, its projection onto a horizontal plane $\mathcal{H}$ containing the common axis of the two actuated wheels being C', as indicated in Fig. 10.17b. Let, moreover, the position vector of C' in a frame fixed to the ground, with origin lying in $\mathcal{H}$, be denoted by $\mathbf{c}$. Additionally, let ω be the scalar angular velocity of the platform about a vertical axis. By virtue of the two-dof motion of this robot, we can control either the velocity $\dot{\mathbf{c}}$ of C—or of C' for that matter—or a combination of ω and a scalar function of $\dot{\mathbf{c}}$ by properly specifying the two joint rates $\dot{\theta}_1$ and $\dot{\theta}_2$. However, we cannot control the two components of $\dot{\mathbf{c}}$ and ω simultaneously.

In order to proceed with the kinematic analysis of the system at hand, we define an orthonormal triad of vectors whose orientation is fixed with respect to the chassis. Let this triad be denoted by $\{\mathbf{i}, \mathbf{j}, \mathbf{k}\}$, with $\mathbf{k}$ pointing in the upward vertical direction. Thus, the velocities $\dot{\mathbf{o}}_i$ of points O_i, for $i = 1, 2$, are given by

$$\dot{\mathbf{o}}_i = r\dot{\theta}_i \mathbf{j}, \quad i = 1, 2 \tag{10.41a}$$

Furthermore, the velocity of C can now be written in two-dimensional form as

$$\dot{\mathbf{c}} = \dot{\mathbf{o}}_i + \omega \mathbf{E}(\mathbf{c} - \mathbf{o}_i), \quad i = 1, 2 \tag{10.41b}$$

with $\mathbf{E}$ defined as in Eq. (5.55). Thus, all vectors of Eq. (10.41b) are two-dimensional. Substituting Eq. (10.41a) into Eq. (10.41b) and subtracting sidewise Eq. (10.41b) for $i = 1$ and for $i = 2$, we derive

$$[r(\dot{\theta}_1 - \dot{\theta}_2) - \omega l]\mathbf{j} = \mathbf{0}_2$$

Hence, the angular velocity ω of line O_1O_2 in planar motion, which is the same as that of the platform, can be readily expressed as

$$\omega = \frac{r}{l}(\dot{\theta}_1 - \dot{\theta}_2) \tag{10.41c}$$

its positive direction being that of $\mathbf{k}$. Upon substitution of Eqs. (10.41a and b) into Eq. (10.41b), we obtain expressions for $\dot{\mathbf{c}}$ in terms of the joint rates, similar to Eqs. (10.41b), for $i = 1, 2$. Furthermore, upon adding sidewise the two expressions thus resulting, we obtain $\dot{\mathbf{c}}$ in the desired form, namely,

$$\dot{\mathbf{c}} = a\frac{r}{l}(\dot{\theta}_1 - \dot{\theta}_2)\mathbf{i} + \frac{r}{2}(\dot{\theta}_1 + \dot{\theta}_2)\mathbf{j} \tag{10.41d}$$

Equations (10.41c and d) express now the differential direct kinematics relations of the robot under study. In compact form, these relations become

$$\mathbf{t} = \mathbf{L}\dot{\boldsymbol{\theta}}_a \tag{10.41e}$$

with the 3×2 matrix $\mathbf{L}$ defined as

$$\mathbf{L} \equiv \begin{bmatrix} r/l & -r/l \\ (ar/l)\mathbf{i} + (r/2)\mathbf{j} & -(ar/l)\mathbf{i} + (r/2)\mathbf{j} \end{bmatrix} \tag{10.41f}$$

Moreover, the *planar twist* $\mathbf{t}$ of the platform and the two-dimensional vector $\dot{\boldsymbol{\theta}}_a$ of actuated joint rates are defined as

$$\mathbf{t} \equiv \begin{bmatrix} \omega \\ \dot{\mathbf{c}} \end{bmatrix}, \quad \dot{\boldsymbol{\theta}}_a \equiv \begin{bmatrix} \dot{\theta}_1 \\ \dot{\theta}_2 \end{bmatrix} \tag{10.41g}$$

Computing the joint rates from the foregoing equations, i.e., solving the associated inverse kinematics problem, is now a trivial task. The inverse kinematics relations are computed below by noticing that Eq. (10.41c) provides a relation for the joint-rate difference. Thus, all we need now is a second equation for the joint-rate sum. By inspection of Eq. (10.41d), it is apparent that we can derive this relation by dot-multiplying both sides of this equation by $\mathbf{j}$, thereby obtaining

$$\dot{\mathbf{c}} \cdot \mathbf{j} = \frac{r}{2}(\dot{\theta}_1 + \dot{\theta}_2) \tag{10.42}$$

The two equations (10.41c) and (10.42) can now be cast into the usual form

$$\mathbf{J}\dot{\boldsymbol{\theta}}_a = \mathbf{K}\mathbf{t} \tag{10.43a}$$

where the two robot Jacobians $\mathbf{J}$ and $\mathbf{K}$ are given below:

$$\mathbf{J} \equiv \begin{bmatrix} 1 & -1 \\ 1 & 1 \end{bmatrix}, \quad \mathbf{K} \equiv \begin{bmatrix} (l/r) & \mathbf{0}^T \\ 0 & (2/r)\mathbf{j}^T \end{bmatrix} \tag{10.43b}$$

Note that $\mathbf{J}$ is a 2×2 matrix, but $\mathbf{K}$ is a 2×3 matrix.

The inverse kinematics relations are readily derived from Eq. (10.43a), namely,

$$\dot{\theta}_1 = \frac{1}{2}\left(\frac{l}{r}\omega + \frac{2}{r}\dot{y}\right)$$

$$\dot{\theta}_2 = -\frac{1}{2}\left(\frac{l}{r}\omega - \frac{2}{r}\dot{y}\right)$$

where $\dot{y} \equiv \dot{\mathbf{c}} \cdot \mathbf{j}$.

Now, in order to complete the kinematic analysis of the robot at hand, we calculate the rates of the unactuated joints, $\dot{\theta}_3$ and $\dot{\psi}$. To this end, let $\boldsymbol{\omega}_i$, for $i = 1, 2, 3$, and $\dot{\mathbf{o}}_3$ denote the three-dimensional angular velocity vector of the ith wheel and the three-dimensional velocity vector of the center of the caster wheel. Likewise, ω_4 denotes the scalar angular velocity of the bracket.

We thus have, for the angular velocity vectors of the two actuated wheels,

$$\begin{aligned} \boldsymbol{\omega}_1 &= -\dot{\theta}_1\mathbf{i} + \omega\mathbf{k} = -\dot{\theta}_1\mathbf{i} + \frac{r}{l}(\dot{\theta}_1 - \dot{\theta}_2)\mathbf{k} \\ &= \begin{bmatrix} -\mathbf{i} + (r/l)\mathbf{k} & -(r/l)\mathbf{k} \end{bmatrix} \begin{bmatrix} \dot{\theta}_1 \\ \dot{\theta}_2 \end{bmatrix} \end{aligned} \tag{10.44a}$$

$$\begin{aligned} \boldsymbol{\omega}_2 &= -\dot{\theta}_2\mathbf{i} + \omega\mathbf{k} = -\dot{\theta}_2\mathbf{i} + \frac{r}{l}(\dot{\theta}_1 - \dot{\theta}_2)\mathbf{k} \\ &= \begin{bmatrix} (r/l)\mathbf{k} & -\mathbf{i} - (r/l)\mathbf{k} \end{bmatrix} \begin{bmatrix} \dot{\theta}_1 \\ \dot{\theta}_2 \end{bmatrix} \end{aligned} \tag{10.44b}$$

In the ensuing derivations, we will need the velocities of the centers of the two actuated wheels, which were derived in Eq. (10.41a). Moreover, the angular velocity of the caster wheel can be readily written in the frame fixed to the bracket, $\{\mathbf{e}_3, \mathbf{f}_3, \mathbf{k}\}$, namely,

$$\boldsymbol{\omega}_3 = \dot{\theta}_3\mathbf{e}_3 + (\omega + \dot{\psi})\mathbf{k} \tag{10.45}$$

with ψ denoting the angle between vectors $\mathbf{j}$ and $\mathbf{e}_3$ of Fig. 10.17a, measured in the positive direction of $\mathbf{k}$, as indicated in the layout of Fig. 10.18.

Note that vector $\mathbf{e}_3$ is parallel to the axis of rolling of the caster wheel, while $\mathbf{f}_3$ is a horizontal vector perpendicular to $\mathbf{e}_3$. These two sets of unit vectors are related by

$$\mathbf{e}_3 = -\sin\psi\mathbf{i} + \cos\psi\mathbf{j} \tag{10.46a}$$

$$\mathbf{f}_3 = -\cos\psi\mathbf{i} - \sin\psi\mathbf{j} \tag{10.46b}$$

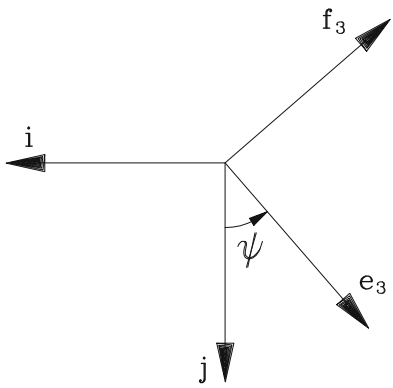

Fig. 10.18 Layout of the unit vectors fixed to the platform and to the bracket

their inverse relations being

$$\mathbf{i} = -\sin\psi\,\mathbf{e}_3 - \cos\psi\,\mathbf{f}_3 \tag{10.46c}$$

$$\mathbf{j} = \cos\psi\,\mathbf{e}_3 - \sin\psi\,\mathbf{f}_3 \tag{10.46d}$$

Furthermore, the velocity of the center of the caster wheel is derived as

$$\dot{\mathbf{o}}_3 = \boldsymbol{\omega}_3 \times r\mathbf{k} = -r\dot{\theta}_3\mathbf{f}_3$$

while the scalar angular velocity of the bracket, ω_4, is given by

$$\omega_4 = \omega + \dot{\psi} = \frac{r}{l}(\dot{\theta}_1 - \dot{\theta}_2) + \dot{\psi} \tag{10.47}$$

In Chap. 12 we shall need $\dot{\mathbf{c}}$ in bracket coordinates. Such an expression is obtained from Eqs. (10.41d) and (10.46c and d), namely,

$$\begin{aligned}\dot{\mathbf{c}} = &[-a\frac{r}{l}(\dot{\theta}_1 - \dot{\theta}_2)\sin\psi + \frac{r}{2}(\dot{\theta}_1 + \dot{\theta}_2)\cos\psi]\mathbf{e}_3 \\ &-[a\frac{r}{l}(\dot{\theta}_1 - \dot{\theta}_2)\cos\psi + \frac{r}{2}(\dot{\theta}_1 + \dot{\theta}_2)\sin\psi]\mathbf{f}_3\end{aligned} \tag{10.48}$$

Expressions for the dependent rates in terms of the independent ones, $\dot{\theta}_1$ and $\dot{\theta}_2$, are readily derived. To this end, we express the velocity of P in two independent forms, one in terms of the velocity of O_3 and the other in terms of the velocity of C, i.e.,

$$\dot{\mathbf{p}} = \dot{\mathbf{o}}_3 + \omega_4\mathbf{k} \times (\mathbf{p} - \mathbf{o}_3) \tag{10.49a}$$

$$\dot{\mathbf{p}} = \dot{\mathbf{c}} + \omega\mathbf{k} \times (-b\mathbf{j}) \tag{10.49b}$$

Upon equating the right-hand sides of the above equations, we obtain a three-dimensional vector equation relating dependent with independent rates, namely,

$$-r\dot{\theta}_3\mathbf{f}_3 + (\omega + \dot{\psi})\mathbf{k} \times (\mathbf{p} - \mathbf{o}_3) = \dot{\mathbf{c}} + b\omega\mathbf{i}$$

where we have recalled the expressions derived above for $\dot{\mathbf{o}}_3$ and ω_4. Further, we rewrite the foregoing equation with the unknown rates, $\dot{\theta}_3$ and $\dot{\psi}$, on the left-hand side, i.e.,

$$-r\dot{\theta}_3\mathbf{f}_3 + \dot{\psi}\mathbf{k} \times (\mathbf{p} - \mathbf{o}_3) = \dot{\mathbf{c}} + b\omega\mathbf{i} - \omega\mathbf{k} \times (\mathbf{p} - \mathbf{o}_3) \tag{10.50}$$

Moreover, we note that, from Fig. 10.17,

$$\mathbf{p} - \mathbf{o}_3 = -d\mathbf{f}_3 + (h - r)\mathbf{k}$$

and hence,

$$\mathbf{k} \times (\mathbf{p} - \mathbf{o}_3) = d\,\mathbf{e}_3$$

Equation (10.50) thus becoming

$$-r\dot{\theta}_3\mathbf{f}_3 + \dot{\psi}d\,\mathbf{e}_3 = \dot{\mathbf{c}} + \omega(b\mathbf{i} - d\,\mathbf{e}_3) \tag{10.51}$$

Now it is a simple matter to solve for $\dot{\theta}_3$ and $\dot{\psi}$ from Eq. (10.51). Indeed, we solve for $\dot{\theta}_3$ by dot-multiplying both sides of the above equation by $\mathbf{f}_3$. Likewise, we solve for $\dot{\psi}$ by dot-multiplying both sides of the same equation by $\mathbf{e}_3$, thus obtaining

$$\begin{aligned} -r\dot{\theta}_3 &= \dot{\mathbf{c}} \cdot \mathbf{f}_3 + \omega b\mathbf{i} \cdot \mathbf{f}_3 \\ d\dot{\psi} &= \dot{\mathbf{c}} \cdot \mathbf{e}_3 + \omega(b\mathbf{i} \cdot \mathbf{e}_3 - d) \end{aligned}$$

Now, by recalling the expressions derived above for ω and $\dot{\mathbf{c}}$, we obtain

$$\begin{aligned} \dot{\mathbf{c}} \cdot \mathbf{f}_3 &= -a\frac{r}{l}(\dot{\theta}_1 - \dot{\theta}_2)\cos\psi - \frac{r}{2}(\dot{\theta}_1 + \dot{\theta}_2)\sin\psi \\ \dot{\mathbf{c}} \cdot \mathbf{e}_3 &= -a\frac{r}{l}(\dot{\theta}_1 - \dot{\theta}_2)\sin\psi + \frac{r}{2}(\dot{\theta}_1 + \dot{\theta}_2)\cos\psi \\ \mathbf{i} \cdot \mathbf{f}_3 &= -\cos\psi, \quad \mathbf{i} \cdot \mathbf{e}_3 = -\sin\psi \end{aligned}$$

Therefore,

$$\dot{\theta}_3 = \alpha\cos\psi(\dot{\theta}_1 - \dot{\theta}_2) + \frac{1}{2}(\sin\psi)(\dot{\theta}_1 + \dot{\theta}_2) \tag{10.52a}$$

$$\dot{\psi} = \rho\left[-(\alpha\sin\psi + \delta)(\dot{\theta}_1 - \dot{\theta}_2) + \frac{1}{2}(\cos\psi)(\dot{\theta}_1 + \dot{\theta}_2)\right] \tag{10.52b}$$

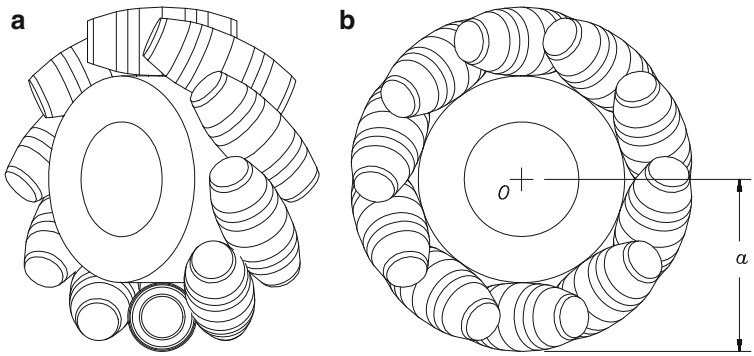

Fig. 10.19 (**a**) The Mekanum Wheel; (**b**) its side view

with the definitions given below:

$$\alpha \equiv \frac{a+b}{l}, \quad \delta \equiv \frac{d}{l}, \quad \rho \equiv \frac{r}{d} \tag{10.53}$$

Hence, if we let $\dot{\boldsymbol{\theta}}_u \equiv [\dot{\theta}_3 \quad \dot{\psi}]^T$ be the vector of *unactuated joint rates*, then we have

$$\dot{\boldsymbol{\theta}}_u = \boldsymbol{\Theta}\dot{\boldsymbol{\theta}}_a \tag{10.54a}$$

with $\boldsymbol{\Theta}$ defined as

$$\boldsymbol{\Theta} \equiv \begin{bmatrix} \alpha\cos\psi + (\sin\psi)/2 & -\alpha\cos\psi + (\sin\psi)/2 \\ \rho[-\alpha\sin\psi + (\cos\psi)/2 - \delta] & \rho[\alpha\sin\psi + (\cos\psi)/2 + \delta] \end{bmatrix} \tag{10.54b}$$

thereby completing the intended kinematic analysis.

10.5.2 Robots with Omnidirectional Wheels

In general, omnidirectional wheels (ODWs) allow for two independent translational motions on the supporting floor and one independent rotational motion about a vertical axis. Based on the shapes of the wheels, moreover, ODWs can be classified into spherical wheels and *Mekanum* wheels, the latter also being known as *ilonators*. Spherical wheels have been extensively investigated in the literature (West and Asada 1995). We focus here on ODWs of the Mekanum type and assume that the robot of interest is equipped with n of these.

The Mekanum wheel bears a set of rollers mounted along the periphery of the wheel hub at a given angle, as shown in Fig. 10.19a. Furthermore, the rollers are shaped so that the wheel appears as circular on its side view, as shown in Fig. 10.19b,

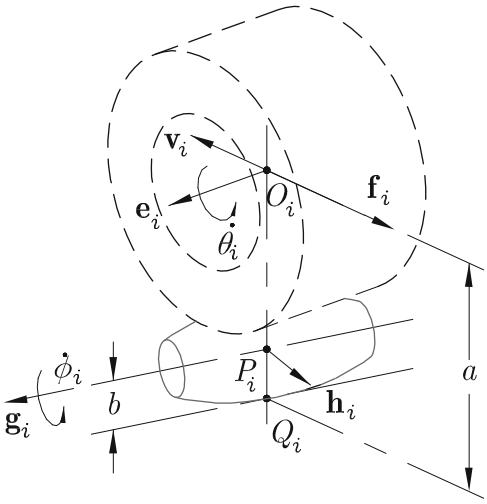

Fig. 10.20 The active roller of the ith wheel

in order to ensure a smooth motion. Pairwise orthogonal unit vectors $\mathbf{e}_i$, $\mathbf{f}_i$ and $\mathbf{g}_i$, $\mathbf{h}_i$ are defined on the middle horizontal planes of the wheel hub and of the roller in contact with the floor, respectively. This roller is termed *active* in the discussion below. Now we aim at finding the kinematic relation between the wheel joint rates $\{\dot{\theta}_i\}_1^n$ and the Cartesian velocity variables of the robot, namely, the scalar angular velocity ω and the two-dimensional velocity vector $\dot{\mathbf{c}}$ of the platform centroid. To this end, we express the velocity $\dot{\mathbf{o}}_i$ of the centroid O_i of the ith wheel in two different forms: first we look at this velocity from the active roller up to the centroid O_i; then, from the platform centroid C to O_i.

If we relate the velocity of O_i with that of the contact point of the active roller with the ground, then we can write, with the aid of Fig. 10.20,

$$\dot{\mathbf{o}}_i = \dot{\mathbf{p}}_i + \mathbf{v}_i \tag{10.55}$$

with $\mathbf{v}_i$ defined as the relative velocity of O_i with respect to P_i. Now let $\boldsymbol{\omega}_h$ and $\boldsymbol{\omega}_r$ denote the angular-velocity vectors of the hub and the roller, respectively, i.e.,

$$\boldsymbol{\omega}_h = \omega\mathbf{k} + \dot{\theta}_i\mathbf{e}_i, \quad \boldsymbol{\omega}_r = \boldsymbol{\omega}_h + \dot{\phi}_i\mathbf{g}_i$$

We thus have

$$\dot{\mathbf{p}}_i = \boldsymbol{\omega}_r \times \overrightarrow{Q_iP_i} = (\omega\mathbf{k} + \dot{\theta}_i\mathbf{e}_i + \dot{\phi}_i\mathbf{g}_i) \times b\mathbf{k}$$

where b is the radius of the rollers at the contact point with ground. In addition, $\dot{\theta}_i$ denotes the rate of the wheel hub, while $\dot{\phi}_i$ denotes that of the active roller, which are positive in the directions of vectors $\mathbf{e}_i$ and $\mathbf{g}_i$, respectively. Hence,

$$\dot{\mathbf{p}}_i = -b(\dot{\theta}_i\mathbf{f}_i + \dot{\phi}_i\mathbf{h}_i) \tag{10.56}$$

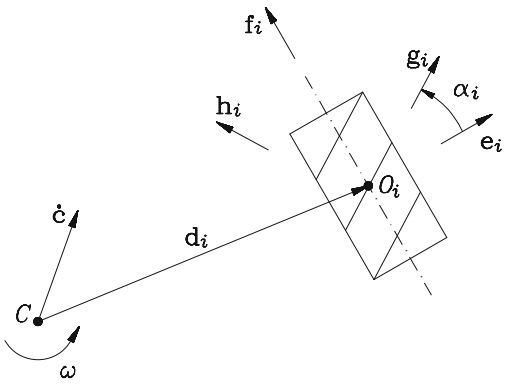

Fig. 10.21 The layout of the ith wheel with respect to the robot platform

Moreover,

$$\mathbf{v}_i = \boldsymbol{\omega}_h \times \overrightarrow{P_i O_i} = (\omega \mathbf{k} + \dot{\theta}_i \mathbf{e}_i) \times (a - b)\mathbf{k}$$

a denoting the height of the axis of the wheel hub, as shown in Fig. 10.19b. Thus,

$$\mathbf{v}_i = -\dot{\theta}_i (a - b)\mathbf{f}_i \tag{10.57}$$

thereby obtaining the desired expression for $\dot{\mathbf{o}}_i$, namely,

$$\dot{\mathbf{o}}_i = -a\dot{\theta}_i \mathbf{f}_i - b\dot{\phi}_i \mathbf{h}_i \tag{10.58}$$

A general layout of the ith ODW with roller axes at an angle α_i with respect to the normal $\mathbf{e}_i$ to the middle vertical plane of the corresponding hub is shown in Fig. 10.21. The subscript i is associated with both the ith wheel and its active roller. Moreover, the velocity $\dot{\mathbf{o}}_i$ of the ith wheel can be expressed in terms of the Cartesian velocity variables, $\dot{\mathbf{c}}$ and ω, as

$$\dot{\mathbf{o}}_i = \dot{\mathbf{c}} + \omega \mathbf{E}\mathbf{d}_i \tag{10.59}$$

where we have used a two-dimensional vector representation, with $\mathbf{d}_i$ defined as the vector directed from point C to the centroid O_i of the hub and $\mathbf{E}$ defined as in Eq. (5.55). Furthermore, since all rollers are unactuated and they rotate idly, the value of $\dot{\phi}_i$ is immaterial to our study. Hence, we eliminate this variable from the foregoing equations, which is done by dot-multiplying both sides of Eq. (10.58) by $\mathbf{g}_i$, normal to $\mathbf{h}_i$, thereby deriving

$$\mathbf{g}_i^T \dot{\mathbf{o}}_i = -a\dot{\theta}_i \mathbf{g}_i^T \mathbf{f}_i$$

But

$$\mathbf{g}_i^T \mathbf{f}_i = \sin \alpha_i$$

Therefore,

$$\mathbf{g}_i^T \dot{\mathbf{o}}_i = -a(\sin\alpha_i)\dot{\theta}_i \tag{10.60}$$

The same multiplication performed on Eq. (10.59) yields

$$\mathbf{g}_i^T \dot{\mathbf{o}}_i = (\mathbf{g}_i^T \mathbf{E}\mathbf{d}_i)\omega + \mathbf{g}_i^T \dot{\mathbf{c}} \tag{10.61}$$

Upon equating the right-hand sides of Eqs. (10.60) and (10.61), we derive the desired relation, namely,

$$-a(\sin\alpha_i)\dot{\theta}_i = \mathbf{k}_i^T \mathbf{t}, \quad i = 1, \ldots, n \tag{10.62}$$

where the three-dimensional vector $\mathbf{k}_i$ is defined as

$$\mathbf{k}_i = \begin{bmatrix} \mathbf{g}_i^T \mathbf{E}\mathbf{d}_i \\ \mathbf{g}_i \end{bmatrix}$$

and the twist vector $\mathbf{t}$ is as defined in Eq. (10.41g). We now define the vector of *wheel rates* $\dot{\boldsymbol{\theta}}$ in the form

$$\dot{\boldsymbol{\theta}} \equiv \begin{bmatrix} \dot{\theta}_1 & \dot{\theta}_2 & \cdots & \dot{\theta}_n \end{bmatrix}^T \tag{10.63}$$

If the n equations of Eq. (10.62) are now assembled, we obtain

$$\mathbf{J}\dot{\boldsymbol{\theta}} = \mathbf{K}t \tag{10.64}$$

where, if we assume that all angles α_i are identical and labeled α, then the $n \times n$ Jacobian $\mathbf{J}$ and the $n \times 3$ Jacobian $\mathbf{K}$ take the forms

$$\mathbf{J} \equiv -a \sin\alpha \mathbf{1} \tag{10.65a}$$

$$\mathbf{K} \equiv \begin{bmatrix} \mathbf{g}_1^T \mathbf{E}\mathbf{d}_1 & \mathbf{g}_1^T \\ \vdots & \vdots \\ \mathbf{g}_n^T \mathbf{E}\mathbf{d}_n & \mathbf{g}_n^T \end{bmatrix} \tag{10.65b}$$

with $\mathbf{1}$ denoting the $n \times n$ identity matrix.

Given Eqs. (10.65a) and (10.65b), the differential inverse kinematics can be resolved as

$$\dot{\boldsymbol{\theta}} = -\frac{1}{a \sin\alpha}\mathbf{K}t \tag{10.66}$$

whence it is apparent that $\sin\alpha$ must be different from zero, i.e., the axes of the rollers must not be parallel to the axis of the hub. If these axes are parallel, then the ODWs reduce to conventional wheels.

10.6 Exercises

10.1 For the parallel manipulator of Fig. 10.2, find the matrix mapping joint forces into wrenches acting on the moving platform, if actuation is supplied through the prismatic joints.

10.2 Show that, if $\det(\mathbf{H})$ of Eq. (10.21) is expanded in the form

$$\det(\mathbf{H}) = \mathbf{H}_1\Delta_1 - \mathbf{H}_2\Delta_2 + \mathbf{H}_3\Delta_3$$

then Δ_1, Δ_2, and Δ_3 are 14th-, 13th-, and 12th-degree polynomials in τ_2, respectively.

10.3 What is the counterpart of a decoupled serial manipulator, as described in Sect. 4.4, of a six-dof parallel manipulator with an architecture similar to that of Fig. 10.2? What is the degree of the characteristic polynomial of that parallel manipulator? Compare this answer with the characteristic polynomial derived in Sect. 4.4.

10.4 We refer to the rolling robot with conventional wheels introduced in Sect. 10.5.1. We would like to study the equivalent concept of manipulability, which here we can call *maneuverability*. This concept refers to the numerical conditioning of the two underlying Jacobian matrices, **J** and **K**, as defined in Eqs. (10.43a and b). Clearly, **J** is isotropic and hence, optimally conditioned. In attempting to determine the condition number of **K**, however, we need to order its singular values from smallest to largest.

(a) Show that the two singular values of **K** are $\sigma_1 = l/r$ and $\sigma_2 = 2/r$. Obviously, an ordering from smallest to largest is impossible because of the lack of dimensional homogeneity.

(b) In order to cope with the dimensional inhomogeneity of matrix **K**, we introduce the characteristic length L, which we define below. First, we redefine the Jacobian **K** in dimensionless form as

$$\mathbf{K} \leftarrow \begin{bmatrix} (l/r) & 0 \\ 0 & 0 \end{bmatrix} \quad \begin{matrix} 0 \\ 2L/r \end{matrix}$$

Now, L is the value that minimizes the condition number of the dimensionless **K**. Show that this value is $l/2$ and that it produces a condition number of unity.

10.5 With reference to the robot of Fig 10.17, assume that the motors are placed rather on the joints associated with variables ψ and θ_3. Under these conditions,

(a) Find the matrix $\mathbf{\Psi}$ mapping array $[\dot{\theta}_3 \quad \dot{\psi}]^T$ into array $[\dot{\theta}_1 \quad \dot{\theta}_2]^T$.
(b) Is it possible to find values of ψ, α, δ, and ρ that will render $\mathbf{\Psi}$ isotropic? If so, which are these values?

10.6 Find an expression for the angular velocity $\dot{\phi}_i$ of the active roller of the ith wheel of the robot with Mekanum wheels introduced in Sect. 10.5.2.

10.7 We refer again to the robot with Mekanum wheels introduced in Sect. 10.5.2. For the case of a three-wheeled robot of this kind, we consider here a design whereby the wheels are equally spaced in a Δ-array. In this array, the centers of the hubs, O_i, lie at the corners of an equilateral triangle of side a; moreover, we assume that $\alpha_i = 90°$, for $i = 1, 2, 3$. Under these conditions, find the characteristic length L of the robot that renders $\mathbf{K}$, as defined in the above-mentioned subsection, dimensionless and of a minimum condition number. Find this minimum as well.

10.8 Find the value of ψ at which the rolling robot of Fig. 10.17 attains a singular configuration. Here, a singularity is understood as a loss of maneuverability in the sense of not being able to drive the unactuated joints by means of the actuated ones. Discuss whether under *reasonable* values of the geometric parameters, this singularity can occur.

10.9 Determine the architecture and the "posture", i.e., the values of the relevant joint variables of the rolling robot of Fig. 10.17 that will render matrix $\mathbf{\Theta}$ isotropic, where $\mathbf{\Theta}$ represents the mapping of actuated joint rates into unactuated ones. Is kinematic isotropy, in this sense, kinematically possible?

10.10 Find a relation among the geometric parameters of the robot of Fig. 10.17 that will allow the steering of the robot along a straight course with the highest possible maneuverability in the sense defined in Exercise 10.8. That is, find a relation among the geometric parameters of this robot that will render $\kappa(\mathbf{\Theta})$ a minimum along a straight course.

10.11 Find the value of ψ under which the robot of Fig. 10.17 performs a maneuver that leaves the midpoint of segment $\overline{O_1 O_2}$ stationary. Under this maneuver, state a relationship among the geometric parameters of the robot that minimizes $\kappa(\mathbf{\Theta})$.

10.12 Upon inversion, Eq. (10.54a) yields

$$\dot{\boldsymbol{\theta}}_a = \mathbf{U}\dot{\boldsymbol{\theta}}_u$$

(a) Find $\mathbf{U}$.
(b) The above equation can be written as

$$\dot{\theta}_1 = u_{13}\dot{\theta}_3 + u_{1\psi}\dot{\psi} \equiv \mathbf{u}_1^T \dot{\boldsymbol{\theta}}_u$$
$$\dot{\theta}_2 = u_{23}\dot{\theta}_3 + u_{2\psi}\dot{\psi} \equiv \mathbf{u}_2^T \dot{\boldsymbol{\theta}}_u$$

The first of the above equations can be integrated if $\mathbf{u}_1$, which is an implicit function of θ_3 and ψ, is the gradient with respect to $\boldsymbol{\theta}_u \equiv [\,\theta_3 \quad \psi\,]^T$ of a scalar function $U_1(\theta_3, \psi)$. Likewise, the second of the above equations can be integrated if a function $U_2(\theta_3, \psi)$ exists, whose gradient with respect to $\boldsymbol{\theta}_u$ is $\mathbf{u}_2$. Further, upon recalling Schwartz's Theorem of multivariable calculus, $\mathbf{u}_i$ is such a gradient if and only if $\nabla \mathbf{u}_i$, i.e., the *Hessian matrix* of U_i with respect to $\boldsymbol{\theta}_u$, is symmetric, for $i = 1, 2$.

Show that the above-mentioned Hessians, for the case at hand, are nonsymmetric, and hence, none of the above differential expressions is integrable. Such expressions are called *nonholonomic*.

Note: To be sure, the above condition is sufficient, but not necessary. It is possible that some individual equations of a system of differential expressions, also called *Pfaffian forms*, are not integrable while the overall system is. An examination of necessary and sufficient conditions for integrability falls beyond the scope of this book. Such conditions are best understood with the aid of the Frobenius Theorem (De Luca and Oriolo 1995) and its analog, the Holonomy Theorem (Ostrovskaya and Angeles 1998).

10.13 For the rolling robot with omnidirectional wheels introduced in Sect. 10.5.2, with a Δ-array, as described in Exercise 10.7, show that the equation yielding the angular velocity of the platform in terms of the wheel rates is integrable, but the equations yielding the velocity of the operation point are not.

10.14 **A holonomic rolling robot.** The robot described in Exercise 10.13 can be rendered holonomic at the expense of one degree of freedom. Show that if the three wheel rates are coordinated, either mechanically or electronically so that

$$\dot{\theta}_1 + \dot{\theta}_2 + \dot{\theta}_3 = 0$$

then the platform is constrained to move under pure translation. When operating in this mode, the robot is holonomic. Find an explicit expression for the position vector $\mathbf{c}$ of the operation point in terms of the wheel angles.